

PCCP

Accepted Manuscript



This is an *Accepted Manuscript*, which has been through the Royal Society of Chemistry peer review process and has been accepted for publication.

Accepted Manuscripts are published online shortly after acceptance, before technical editing, formatting and proof reading. Using this free service, authors can make their results available to the community, in citable form, before we publish the edited article. We will replace this *Accepted Manuscript* with the edited and formatted *Advance Article* as soon as it is available.

You can find more information about *Accepted Manuscripts* in the [Information for Authors](#).

Please note that technical editing may introduce minor changes to the text and/or graphics, which may alter content. The journal's standard [Terms & Conditions](#) and the [Ethical guidelines](#) still apply. In no event shall the Royal Society of Chemistry be held responsible for any errors or omissions in this *Accepted Manuscript* or any consequences arising from the use of any information it contains.

Intermolecular Vibrational Energy Transfers in Liquids and Solids

Hailong Chen, Xiewen Wen, Xunmin Guo, Junrong Zheng*

Department of Chemistry, Rice University, Houston, TX

*To whom correspondence should be addressed: junrong@rice.edu

Abstract

Resonant and nonresonant intermolecular vibrational energy transfers in KSCN/KSC¹³N/KS¹³C¹⁵N aqueous and DMF solutions and crystals are studied. Both energy-gap and temperature dependent measurements reveal some surprising results, e.g. inverted energy-gap dependent energy transfer rates and opposite temperature dependences of resonant and nonresonant energy transfer rates. Two competing mechanisms are proposed to be responsible for the experimental observations. The first one is the dephasing mechanism of which the measured energy transfer rate originates from the dephasing of the energy donor/acceptor coherence, and the second one is the phonon-compensation mechanism derived from the second order perturbation. It is found that both the nonresonant energy transfers in the liquids and resonant energy transfers in both liquids and solids can be well described by the first mechanism. The second mechanism explains the nonresonant energy transfers in one series of the solid samples very well.

1. Introduction

Vibration, as one of the three basic molecular motions, is an indispensable part of chemical transformations. Vibrational energy transfers, are therefore involved in all chemical bond transformation activities in condensed phases, and play critical roles in many important phenomena in various fields, e.g. the heat transport, the chemical reaction energy dissipations, the electronic excitation energy conversions and dissipations (e.g. in solar cells, and photosynthetic systems), and the trans-membrane cell signaling. The significance of vibrational energy transfers has long been well recognized, and research on them in condensed phases started several decades ago.¹⁻¹¹ However, the quantitative description of intermolecular vibrational energy transfers remains a grand challenge, as intermolecular energy transfers are typically accompanied by intramolecular energy relaxations and many mechanisms can play roles simultaneously.¹²⁻¹⁵

Recently we conducted a series of intermolecular vibrational energy transfers experiments in liquids,¹⁶⁻²² and found that the intermolecular energy transfers observed can be described by an equation¹⁸ derived from the well-known correlation formalism vibrational relaxation theory.^{4, 14, 23} However, the results are difficult to be rationalized with the phonon-compensation mechanism.¹⁵

In this work, we performed comprehensive experiments to investigate resonant and nonresonant intermolecular vibrational energy transfers among the nitrile stretches (CN, ¹³CN, and ¹³C¹⁵N) in the KSCN/KS¹³CN/KS¹³C¹⁵N aqueous and DMF solutions and crystalline samples. From the experiments, we observed opposite temperature dependences for the nonresonant and resonant energy transfers, and inverted energy-gap dependences of nonresonant energy transfer rates. The surprising results cannot be fully

explained by either the equation used in our previous work¹⁸ or the phonon compensation mechanism derived from the 1st order perturbation¹⁵. Summarizing all our experimental results reported in the current and previous work,^{18,19,24} we propose that the experimentally observed intermolecular vibrational energy transfers result from two competing mechanisms. The first one is the dephasing mechanism (similar to the Forster energy transfer type)²⁴ in which the observed energy transfer rate is determined by the dephasing of the energy donor/acceptor coherence. This mechanism gives rise to both resonant and nonresonant energy transfers. The other is the phonon-compensation mechanism derived from the second order perturbation (the second order coupling matrix) approach which is only responsible for nonresonant energy transfers.

2. Experiments

One ps amplifier and one fs amplifier are synchronized with the same seed pulse. The ps amplifier pumps an OPA to generate ~ 0.8 ps (varying from 0.7~0.9 ps as a function of frequency) mid-IR pulses with a bandwidth 10~35 cm^{-1} in a frequency range tunable from 400 cm^{-1} to 4000 cm^{-1} with energy 1 ~ 40 $\mu\text{J}/\text{pulse}$ (1 ~ 10 $\mu\text{J}/\text{pulse}$ for 400 cm^{-1} to 900 cm^{-1} and >10 $\mu\text{J}/\text{pulse}$ for higher frequencies) at a rate of 1 KHz. The $\sim 1.5\text{W}$ output from the fs amplifier is used to generate a high-intensity mid-IR and terahertz super-continuum pulse with a duration <100 fs in the frequency range from <10 cm^{-1} to >3500 cm^{-1} at 1 KHz. In nonlinear IR experiments, the ps IR pulse is the excitation pulse (the excitation power is adjusted based on need and the interaction spot varies from 100 to 500 microns). The super-continuum pulse is the detection beam which is frequency resolved by a spectrograph (resolution is 1~3 cm^{-1} dependent on the frequency) yielding the detection axis of a 2D IR spectrum. Two polarizers are introduced into the

detection beam path to selectively measure the parallel or perpendicular polarized signal relative to the excitation beam. The dependence of the rotation-free signal $P_{life} = P_{\parallel} + 2 \times P_{\perp}$ upon the pump-probe delay, where P_{\parallel}, P_{\perp} are parallel and perpendicular data respectively, determines the vibrational lifetime. The waiting time dependent anisotropy values are obtained from $r(t) = (P_{\parallel} - P_{\perp}) / (P_{\parallel} + 2 \times P_{\perp})$. That the sample is isotropic within the laser focus spot is verified by measuring the initial anisotropy values of the sample as it is rotated relative to the polarization of the excitation beam. The THz spectra were taken from a home-built ABCD THz detection system,²⁵ and the Raman spectra were taken from a commercial Raman spectrometer. In the analyses of reorientation dynamics and vibrational energy transfer kinetics, the heat effects from the thiocyanate vibrational relaxations which are very small were removed, following the procedure described in our previous publication¹⁶: the heat signal is assumed to grow with time constants slightly slower than the lifetimes of vibrational excitations of which the relaxation generates heat. The maximum amplitude of heat signal is the transient signal at very long waiting times when most vibrational excitations have relaxed. The time dependent heat signal calculated is then subtracted from the transient signal.

Unless specified, chemicals were purchased from Sigma–Aldrich and used without further purification. $KS^{13}C^{15}N$ and $KS^{13}CN$ were purchased from Cambridge Isotope Laboratory. The solid samples were thin films of polycrystalline $KSCN/KS^{13}C^{15}N$ mixed crystals blended with ~50 wt% PMMA (Poly(methyl methacrylate)). The function of PMMA was to suppress scattered light. In the low temperature measurements, the samples were placed in a Janis cryostat under vacuum. In

the high temperature measurements, the samples were placed in a Harrick Scientific temperature control cell.

3. Theoretical background

The theory of energy transfers between molecules and energy relaxations in condensed phases has been addressed by a number of authors.^{4, 15, 23, 24, 26-38} There are two possible limiting cases of vibrational energy transfers: $V \ll \tau^{-1}$ and $V \geq \tau^{-1}$ where V is the donor/acceptor coupling strength and τ^{-1} is the homogeneous dephasing linewidth of the donor or the acceptor. Most of the present work will be concerned with the first case of resonant and near resonant energy transfers. Based on the listed pioneering work, the derivations with some phenomenological descriptions leading to energy transfer rate equations that serve as foundation to explain our experimental results are provided in the following.

3.1 Dephasing Mechanism

The vibrational energy transfer equation of the dephasing mechanism³⁶⁻³⁹ can be derived from the coupled donor/acceptor pair, following our previous work⁴⁰ with some modifications. The derivation leads to an equation of which all parameters can be experimentally quantitatively determined. The system state can be expressed as

$$|\psi\rangle = c_1(t)e^{-i\omega_D t} |D=1, A=0\rangle + c_2(t)e^{-i\omega_A t} |D=0, A=1\rangle, \quad \text{eq.1}$$

where ω_D and ω_A are the 0-1 transition frequency of the donor (D) and the acceptor (A), respectively. $|D=1, A=0\rangle$ is the donor state where the donor is at the 1st excited state and the acceptor is at the ground state. $|D=0, A=1\rangle$ is the acceptor state where the donor is at the ground state and the acceptor is at the 1st excited state. $c_1(t)$ and $c_2(t)$ are the

coefficients of these two states with $|c_1(t)|^2 + |c_2(t)|^2 \equiv 1$. The coupling between the two states is $V = \frac{\langle D=1, A=0 | H | D=0, A=1 \rangle}{\hbar} = \frac{\langle D=0, A=1 | H | D=1, A=0 \rangle}{\hbar}$ where H is the system Hamiltonian. Substituting eq.1 into the time dependent Schrödinger equation with the initial condition $c_1(0) = 1; c_2(0) = 0$, one can obtain

$$c_1(t) = e^{\frac{1}{2}i\Delta\omega t} \left[\cos \left[\frac{t}{2} \sqrt{(\Delta\omega)^2 + 4V^2} \right] - i \frac{\Delta\omega \sin \left[\frac{t}{2} \sqrt{(\Delta\omega)^2 + 4V^2} \right]}{\sqrt{(\Delta\omega)^2 + 4V^2}} \right] \quad \text{eq.2}$$

$$c_2(t) = \frac{2Ve^{-\frac{1}{2}i\Delta\omega t} \sin \left(\frac{t}{2} \sqrt{(\Delta\omega)^2 + 4V^2} \right)}{\sqrt{(\Delta\omega)^2 + 4V^2}}, \quad \text{eq.3}$$

where $\Delta\omega = \omega_A - \omega_D$. Here we propose that the coherence between the donor and acceptor states is terminated by an abrupt dephasing event which is random and therefore follows the 1st order kinetics. After the dephasing event, the system stays in the acceptor state with a probability $|c_2(t_c)|^2$. The ensemble average probability on the acceptor state

for a dephasing period τ is $P = \int_0^{\infty} |c_2(t_c)|^2 p(t_c) dt_c$, where $p(t_c) = \tau^{-1} e^{-t_c/\tau}$ is the

probability of dephasing at time t_c with $\int_0^{\infty} p(t_c) dt_c = 1$.³⁹ The acceptor state growth rate

constant is therefore

$$k_p = \frac{P}{\tau} = 2V^2 \frac{1}{(\Delta\omega)^2 + 4V^2 + \tau^{-2}}. \quad \text{eq.4}$$

The growth rate constant $k_p = k_{DA} + k_{AD}$, where k_{DA} is the energy transfer rate constant from the donor state to the acceptor state and k_{AD} is the reverse constant, can be

derived from the kinetic scheme: $D \xrightleftharpoons[k_{AD}]{k_{DA}} A$, where $k_{DA} = e^{\frac{\Delta\omega}{RT}} k_{AD}$ determined by the detailed balance principle and the kinetic solution is $D(t) = \frac{1}{2} e^{-(k_{DA}+k_{AD})t} + \frac{1}{2}$ and $A(t) = -\frac{1}{2} e^{-(k_{DA}+k_{AD})t} + \frac{1}{2}$ with the initial condition $D(0)=1, A(0)=0$. Therefore, the energy transfer rate constant from the donor state to the acceptor state is

$$k_{DA} = \frac{2}{1 + e^{\frac{\Delta\omega}{RT}}} V^2 \frac{\frac{1}{\tau}}{(\Delta\omega)^2 + 4V^2 + \tau^{-2}}. \quad \text{eq.5}$$

Eq.5 is the energy transfer rate equation of the dephasing mechanism. It requires $V < \tau^{-1}$. For $V > \tau^{-1}$, the coherent energy transfer mechanism will dominate, i.e. a donor-acceptor exciton will persist.²⁴ In all the experiments reported here, $V < \tau^{-1}$. All the parameters of eq.5 are experimentally accessible and therefore it can be quantitatively experimentally tested. An equation similar to eq.5 can also be derived from the correlation formalism with the assumption that the vibrational coupling correlation function is a single exponential.^{4, 18}

If the 0-1 dephasing of the donor is uncorrelated to the 0-1 dephasing of the acceptor, another equation similar to eq.5 can be derived in the frequency domain. Under the weak coupling limit, the probability at the acceptor state can be obtained by simplifying eq.3 or directly from the 1st order perturbation:

$$|c_2(t)|^2 = \frac{4V^2 \sin^2\left(\frac{\Delta\omega}{2} t\right)}{(\Delta\omega)^2}. \quad \text{eq.6}$$

Both the donor and acceptor 0-1 transitions are assumed to be homogeneously broadened so that both 0-1 transition lineshapes are Lorentzian with line widths τ_D and τ_A respectively. The probability of the donor at a frequency ω_1 is $\frac{1}{\pi} \frac{\tau_D^{-1}}{(\omega_1 - \omega_D)^2 + \tau_D^{-2}}$, and that of the acceptor at a frequency ω_2 is $\frac{1}{\pi} \frac{\tau_A^{-1}}{(\omega_2 - \omega_A)^2 + \tau_A^{-2}}$. The experimentally

observed energy transfer is the sum of the transfers among all these possible donor and acceptor frequencies. Therefore, the donor/acceptor energy transfer rate constant is

$$k_{DA} = \frac{1}{1 + e^{\frac{\Delta\omega}{RT}}} \times \frac{1}{t} \times \int_{-\infty}^{\infty} \int_{-\infty}^{\infty} \frac{1}{\pi} \times \frac{\tau_D^{-1}}{(\omega_x - \omega_D)^2 + \tau_D^{-2}} \times \frac{1}{\pi} \times \frac{\tau_A^{-1}}{(\omega_\Lambda + \omega_x - \omega_A)^2 + \tau_A^{-2}} \times |c_2(t, \omega_\Lambda)|^2 d\omega_x d\omega_\Lambda. \quad \text{eq.7}$$

Substituting eq.6 into eq.7 and simplifying it, we obtain

$$k_{DA} = \frac{1}{1 + e^{\frac{\Delta\omega}{RT}}} \times \frac{1}{t} \times \int_{-\infty}^{\infty} \frac{1}{\pi} \times \frac{\tau_A^{-1} + \tau_D^{-1}}{[\omega_\Lambda - (\omega_A - \omega_D)]^2 + (\tau_A^{-1} + \tau_D^{-1})^2} \times \frac{t}{2} \times \frac{4V^2 \sin^2\left(\frac{\omega_\Lambda t}{2}\right)}{\left(\frac{\omega_\Lambda t}{2}\right)^2} d\left(\frac{\omega_\Lambda t}{2}\right). \quad \text{eq.8}$$

Eq.8 can be transformed into

$$k_{DA} \cong \frac{2V^2}{1 + e^{\frac{\Delta\omega}{RT}}} \times \frac{1}{\pi} \times \frac{\tau_A^{-1} + \tau_D^{-1}}{(\omega_A - \omega_D)^2 + (\tau_A^{-1} + \tau_D^{-1})^2} \int_{-\infty}^{\infty} \frac{\sin^2\left(\frac{\omega_\Lambda t}{2}\right)}{\left(\frac{\omega_\Lambda t}{2}\right)^2} d\left(\frac{\omega_\Lambda t}{2}\right). \quad \text{eq.9}$$

The integration in eq.9 is π , so that eq.9 becomes

$$k_{DA} = \frac{2V^2}{1 + e^{\frac{\Delta\omega}{RT}}} \frac{\tau_A^{-1} + \tau_D^{-1}}{(\omega_A - \omega_D)^2 + (\tau_A^{-1} + \tau_D^{-1})^2}. \quad \text{eq.10}$$

Eq.10 is the weak coupling limit of eq.5 for the uncorrelated D/A dephasing case. It is similar to the electronic energy transfer rate equation of the hopping mechanism.²⁴ Comparing eq.5 and eq.10, we can see that if the 0-1 transition dephasings of the donor and acceptor are uncorrelated, the energy transfer dephasing time τ in eq.5 can be

obtained from $\tau^{-1} = \tau_A^{-1} + \tau_D^{-1}$. For most cases, the intermolecular vibrational energy transfers that can be experimentally observed are expected to occur within the distance smaller than 1nm because of the relatively small vibrational transition dipole moments (0.2~0.5D) and short vibrational lifetimes (a few to hundreds of ps). Within such short distances, the molecular factors, e.g. the electric field fluctuation, that cause the donor to dephase, must also affect the dephasing of the acceptor in a certain way, vice versa. In other words, the dephasings of the donor and acceptor are correlated. For the correlated cases, the energy transfer dephasing time τ must be longer than that of the uncorrelated case. How long τ can be is dependent on the detailed correlation, which cannot be directly obtained from a single experiment. However, according eq.5, τ can be obtained by measuring the energy transfer rates with different energy gaps ($\Delta\omega$).

The physical picture behind eq.5 can be deduced from the above derivations for both eqs.5&10: the energy transfer rate described by eq.5 is determined by the resonant energy transfer of the portions of donor and acceptor at the same frequencies. (Different from the situation in eq.10, the frequency overlap range is smaller in eq.5 because of the correlated dephasings). For a donor and an acceptor with different central frequencies (ω_D and ω_A), the dephasing events inevitably cause the donor and acceptor to have some same frequencies with certain probabilities. At these same frequencies, the donor and acceptor transfer energy resonantly, and then the acceptor which carries the transferred energy may change its frequencies because of dephasing, spectral diffusion or chemical exchange. Such a resonant energy transfer process contributes to the overall experimentally observed nonresonant energy transfers. A smaller central frequency difference results in a larger frequency overlap and a faster energy transfer.

Similar to a previous theory,³⁶⁻³⁸ eq.5 also predicts a non-monotonic dephasing time dependence of energy transfer rate. When the dephasing is fast (τ^{-1} is larger than the energy gap $\Delta\omega$ between the donor and acceptor), the energy transfer rate is roughly proportional to τ and therefore the energy transfer is slower with a faster dephasing. When the dephasing is slow (τ^{-1} is smaller than the energy gap $\Delta\omega$ between the donor and acceptor), the energy transfer rate is roughly inversely proportional to τ . The energy transfer is faster with a faster dephasing. The physical pictures behind such a non-monotonic behavior can be understood from both derivations in the time and frequency domains described above: (A) When the gap is much larger than the dephasing width (τ^{-1}), the energy transfer rate is limited by the probability for the donor and acceptor to be on resonance. A faster dephasing causes a larger probability for the donor and acceptor to be on resonance and therefore a faster transfer rate. (B) When the dephasing width is much larger than the gap, which implies that the donor and acceptor have significant energy overlaps and the chance for them to be on resonance is large, the energy transfer rate is limited by the donor/acceptor coherence time. A longer coherence leads to a larger probability of the excitation on the acceptor state and thus a faster energy transfer. A faster dephasing causes a shorter donor/acceptor coherence and thus a slower energy transfer. One extreme case of situation (B) is the resonant energy transfer where the donor and acceptor have the same energy.

If the central frequency difference is large and the dephasing time is long, the probability for the donor and acceptor to have the same frequency is very small and the nonresonant energy transfer predicted by eq.5 is very slow. Under this situation, another energy transfer mechanism, the phonon compensation nonresonant energy transfer

mechanism, can be important. Similar to the nonlinear optical effect that one photon can split into several photons or several photons can combine into one photon, energy can directly transfer nonresonantly from the donor to the acceptor of a different frequency by emitting or absorbing photons into or from the environments to conserve energy. We call the nonresonant energy transfer processes as the phonon compensation mechanism. In this work, we will only discuss the process of emitting or absorbing one photon (phonon), or the so called “cubic” process.¹⁵ Processes involving more phonons are typically slower and we expect that it is difficult to experimentally observe these slow processes as many competing energy transfer pathways (e.g. intramolecular relaxations) are much faster.

Before we go to the phonon compensation mechanism, one issue needs to be discussed. In addition to the dephasing process that can cause some frequency overlap, inhomogeneous broadening can also do the same thing. In a system in a condensed phase, the vibrational line width is typically the results of both processes. For a very inhomogeneous system, the decomposition of a peak into several homogeneous sub-components is needed before applying eq.5. In reality, as determined by 2D IR, most room temperature liquid samples that have been measured contain only 10% to 30% inhomogeneous broadening contribution.⁴¹⁻⁴⁶ Such an amount of inhomogeneous broadening can introduce a similar amount of uncertainty into the determined energy transfer rate by directly using eq.5. However, because the energy transfer dephasing time τ in eq.5 is an effective (average) parameter determined by the energy-gap dependent experiments rather than from the linear absorption lineshapes, the uncertainty is expected to be smaller than the contribution of inhomogeneous broadening to the total line width.

In addition, the energy transfer dephasing time τ determined by this method already contains the contribution of spectral diffusion.

3.2 Phonon Compensation Mechanism

Nonresonant vibrational relaxations or transfers compensated with phonons from the bath were theoretically described previously.^{15, 47, 48} For the one-phonon process (the cubic process) of nonresonant intermolecular vibrational energy transfers, different from the previous work¹⁵ where nonresonant energy transfers were treated as a process directly from the donor state to the acceptor state, the derivation in the following requires virtual intermediate states between the donor and acceptor states. The difference in mechanism results in a different energy transfer rate equation.

The derivation follows the theory of nonresonant electronic energy transfers of impurities in solids.³² According to the golden rule, the transition probability per unit time for excitation transfer to take place is

$$k_{fi} = \frac{2\pi}{\hbar} |W_{fi}|^2 \rho(E_{fi}), \quad \text{eq.11}$$

where W_{fi} is the coupling matrix element, and $\rho(E)$ is the density of states. The coupling matrix can be expanded to the second-order (higher orders which may require more than one phonons are omitted)

$$W_{fi} = \langle f | H' | i \rangle + \sum_m \frac{\langle f | H' | m \rangle \langle m | H' | i \rangle}{E_i - E_m}, \quad \text{eq.12}$$

where $|i\rangle$ and $|f\rangle$ are the initial and final states, respectively, and $|m\rangle$ denotes all the possible intermediate state. E_i and E_m are the total energy of states $|i\rangle$ and $|m\rangle$ respectively. The coupling Hamiltonian H' consists of direct interaction between donor

and acceptor H_{DA} (e.g. dipole-dipole interaction if the distance is sufficiently large) and the coupling between the system (energy donor and acceptor) and the phonons $H_{ph}(D)$,

$$H_{ph}(A):$$

$$H' = H_{DA} + H_{ph}(D) + H_{ph}(A). \quad \text{eq.13}$$

We have the initial state where the donor D is at its first excited state D^* , the acceptor A is at the ground state A , and the phonon state is n_q

$$|i\rangle = |D^*, A, n_q\rangle, \quad \text{eq.14}$$

and the final state where the donor D is at the ground state D , the acceptor A is at its first excited state A^* , and the phonon state is $n_q \pm 1$

$$|f\rangle = |D, A^*, n_q \pm 1\rangle, \quad \text{eq.15}$$

with equal energy E_i . The energy gap between the donor and acceptor $\Delta E = E_D - E_A$ is made up by one phonon, and the upper and lower signs designate phonon emission $\Delta E > 0$ and absorption $\Delta E < 0$, respectively. The two possible intermediate states are

$$|m_1\rangle = |D^*, A, n_q \pm 1\rangle, \quad \text{eq.16}$$

$$|m_2\rangle = |D, A^*, n_q\rangle. \quad \text{eq.17}$$

with the energy $E_i + \Delta E$ and $E_i - \Delta E$ respectively. \mathbf{q} denotes the wave vector of the phonon, with the energy $\hbar \cdot \omega(\mathbf{q}) = |\Delta E|$.

The first order coupling matrix element is negligibly small, as

$$\begin{aligned}
\langle f|H|i\rangle &= \langle D, A^*, n_q \pm 1 | H_{DA} + H_{ph}(D) + H_{ph}(A) | D^*, A, n_q \rangle \\
&= \langle D, A^*, n_q \pm 1 | H_{DA} | D^*, A, n_q \rangle + \langle D, A^*, n_q \pm 1 | H_{ph}(D) | D^*, A, n_q \rangle + \langle D, A^*, n_q \pm 1 | H_{ph}(A) | D^*, A, n_q \rangle \\
&= \langle D, A^* | H_{DA} | D^*, A \rangle \langle n_q \pm 1 | n_q \rangle + \langle n_q \pm 1 | H_{ph}(D) | n_q \rangle \langle D, A^* | D^*, A \rangle + \langle n_q \pm 1 | H_{ph}(A) | n_q \rangle \langle D, A^* | D^*, A \rangle \\
&= \langle D, A^* | H_{DA} | D^*, A \rangle \times 0 + \langle n_q \pm 1 | H_{ph}(D) | n_q \rangle \times 0 + \langle n_q \pm 1 | H_{ph}(A) | n_q \rangle \times 0 \\
&= 0
\end{aligned} \tag{eq.18}$$

The second order matrix element can be expanded into

$$\begin{aligned}
&\sum_m \frac{\langle f|H|m\rangle \langle m|H|i\rangle}{E_i - E_m} \\
&= \frac{\langle D, A^* | H_{DA} | D^*, A \rangle \langle D^*, n_q \pm 1 | H_{ph}(D) | D^*, n_q \rangle + \langle A, n_q \pm 1 | H_{ph}(A) | A, n_q \rangle}{-\Delta E} \\
&+ \frac{\langle D, n_q \pm 1 | H_{ph}(D) | D, n_q \rangle + \langle A^*, n_q \pm 1 | H_{ph}(A) | A^*, n_q \rangle \langle D, A^* | H_{DA} | D^*, A \rangle}{\Delta E}
\end{aligned} \tag{eq.19}$$

The matrix elements in eq.19 can be written as

$$\begin{aligned}
\langle D, A^* | H_{DA} | D^*, A \rangle &= V \\
\langle D, n_q \pm 1 | H_{ph}(D) | D, n_q \rangle &= g_D(s, q) \cdot \langle n_q \pm 1 | (b_{s,q}^\dagger + b_{s,-q}) | n_q \rangle \cdot \exp(\mp i\mathbf{q} \cdot \mathbf{r}_D) \\
\langle A, n_q \pm 1 | H_{ph}(A) | A, n_q \rangle &= g_A(s, q) \cdot \langle n_q \pm 1 | (b_{s,q}^\dagger + b_{s,-q}) | n_q \rangle \cdot \exp(\mp i\mathbf{q} \cdot \mathbf{r}_A) \\
\langle D^*, n_q \pm 1 | H_{ph}(D) | D^*, n_q \rangle &= e_D(s, q) \cdot \langle n_q \pm 1 | (b_{s,q}^\dagger + b_{s,-q}) | n_q \rangle \cdot \exp(\mp i\mathbf{q} \cdot \mathbf{r}_D) \\
\langle A^*, n_q \pm 1 | H_{ph}(A) | A^*, n_q \rangle &= e_A(s, q) \cdot \langle n_q \pm 1 | (b_{s,q}^\dagger + b_{s,-q}) | n_q \rangle \cdot \exp(\mp i\mathbf{q} \cdot \mathbf{r}_A), \tag{eq.20}
\end{aligned}$$

where $g_i(s, q)$ and $e_i(s, q)$ ($i = D, A$) denote the coupling to the phonon of wave vector \mathbf{q} (branch s) for the ground state and 1st excited state, respectively. $b_{s,q}^\dagger$, $b_{s,-q}$ are the phonon creation and annihilation operators. \mathbf{r}_D and \mathbf{r}_A are the position vectors of donor and acceptor. Inserting eqs.18~20 into eq.12, one can obtain

$$\begin{aligned}
W_{fi}(\mathbf{q}) &= \frac{V}{-\Delta E} \cdot \langle n_q \pm 1 | (b_{s,q}^\dagger + b_{s,-q}) | n_q \rangle \cdot [e_D(s, q) \cdot \exp(\mp i\mathbf{q} \cdot \mathbf{r}_D) + g_A(s, q) \cdot \exp(\mp i\mathbf{q} \cdot \mathbf{r}_A)] \\
&+ \frac{V}{\Delta E} \cdot \langle n_q \pm 1 | (b_{s,q}^\dagger + b_{s,-q}) | n_q \rangle \cdot [g_D(s, q) \cdot \exp(\mp i\mathbf{q} \cdot \mathbf{r}_D) + e_A(s, q) \cdot \exp(\mp i\mathbf{q} \cdot \mathbf{r}_A)]
\end{aligned} \tag{eq.21}$$

We define $\mathbf{r} = \mathbf{r}_A - \mathbf{r}_D$ as the distance vector between the donor and acceptor. If the donor and acceptor have very similar molecular properties, $g_D(s, q) \cong g_A(s, q)$ and $e_D(s, q) \cong e_A(s, q)$. We define $V_{ph}(s, q) = g_D(s, q) - e_D(s, q) = g_A(s, q) - e_A(s, q)$. Under the conditions, eq.21 can be rewritten as

$$W_{fi}(\mathbf{q}) = \frac{V}{\Delta E} \cdot \langle n_{\mathbf{q}} \pm 1 | (b_{s,q}^\dagger + b_{s,-q}) | n_{\mathbf{q}} \rangle \cdot V_{ph}(s, q) \cdot \exp(\mp i\mathbf{q} \cdot \mathbf{r}_A) \cdot [\exp(\pm i\mathbf{q} \cdot \mathbf{r}) - 1]. \quad \text{eq.22}$$

The phonon transition term is

$$\langle n_{\mathbf{q}} \pm 1 | (b_{s,q}^\dagger + b_{s,-q}) | n_{\mathbf{q}} \rangle = \begin{cases} \sqrt{n(s, q) + 1} \\ \sqrt{n(s, q)} \end{cases} \text{ for } \begin{cases} \text{emission} \\ \text{absorption} \end{cases}, \quad \text{eq.23}$$

where $n(s, q) = n(\Delta E, T) = [\exp(|\Delta E|/k_B T) - 1]^{-1}$ is the Boson thermal occupation number, and k_B is Boltzmann's constant. Inserting eqs.22~23 into eq.11, one can obtain the energy transfer rate constant from the initial state to the final state

$$k'_{fi} = \frac{2\pi}{\hbar} \cdot \frac{|V|^2}{\Delta E^2} \cdot \rho_{eff}(\Delta E) \cdot (n(\Delta E, T) + 1) \quad \text{eq.24}$$

for the emission process ($\Delta E > 0$), and

$$k'_{fi} = \frac{2\pi}{\hbar} \cdot \frac{|V|^2}{\Delta E^2} \cdot \rho_{eff}(\Delta E) \cdot n(\Delta E, T) \quad \text{eq.25}$$

for the absorption process ($\Delta E < 0$), where

$$\rho_{eff}(\Delta E) = \sum_s |V_{ph}(s, q)|^2 \cdot |\exp(i\mathbf{q} \cdot \mathbf{r}) - 1|^2 \cdot \rho_s(\Delta E)$$

is the effective phonon density of states weighted by the coupling parameter difference. Eqs.24&25 are the vibrational energy transfer rate equations of the one-phonon compensation mechanism. The essential difference between these equations and the equations in the previous theory assuming the

direct energy transfer from the donor to acceptor¹⁵ is that in eqs.24&25 there is a term ΔE^2 in the denominator.

From the derivation, we can see that a few conditions are required for the energy transfer through this mechanism to be nontrivial. The first one is that the density of states $\rho_s(\Delta E)$ must be reasonably large. The second one is that the coherence term $|\exp(i\mathbf{q}\cdot\mathbf{r}) - 1|^2$ must be nonzero. The physical picture behind this term is that the donor and the acceptor must be so far away that the modulations of phonon on them are different. This condition can be approximately fulfilled for nonresonant vibrational energy transfers with gapes smaller than RT ($\sim 200 \text{ cm}^{-1}$ at room temperature) because both the phonon wavelength and the donor/acceptor distance are at the scale of a few angstroms. The third one is that $|V_{ph}(s, q)|^2$ must be non-zero. In other words, it requires a difference in the couplings of a phonon to the vibrational excited state and the ground state of the same molecule.

3.3 Comparisons between the Two Mechanisms

3.3.1 The Energy Gap Dependence

One major difference between the two mechanisms is that in the dephasing mechanism the energy transfer is slower with a larger energy gap, but in the phonon compensation mechanism this is not necessarily the case. As described by eq.5, for nonresonant energy transfers with the energy gap ($\Delta\omega$) larger than the dephasing width (τ^{-1}), the energy transfer rate constant becomes approximately inversely proportional to the square of energy gap because the coupling strength (V) and dephasing time (τ) are hardly affected by the relatively small energy gap (e.g. $<200 \text{ cm}^{-1}$ at RT). However, according to eqs.24&25, the energy transfer rate is not only determined by the energy gap,

but also by the phonon density of states ($\rho_s(\Delta E)$) and the phonon/system coupling ($V_{ph}(s, q)$) all of which are sensitive to the energy gap. Dependent on the detailed values of these two parameters, the energy transfer rates with two different energy gaps can be the same or different in either way. Experimentally, the difference in the energy gap dependences of the two mechanisms can be tested.

3.3.2 The Temperature Dependence

The energy transfer rates from both mechanisms are temperature dependent. Here we assume that the direct donor/acceptor vibrational coupling (e.g. transition dipole/transition dipole interaction) is hardly affected by the temperature change if no phase transition or chemical transformation occurs. In the dephasing mechanism (eq.5), the temperature change causes the dephasing time τ to change. Typically, at a higher temperature, molecular motions are faster and the dephasing time is shorter. According to eq.5, for the resonant energy transfer, the rate will become slower at a higher temperature, but for a nonresonant energy transfer with the energy gap ($\Delta\omega$) larger than the dephasing width (τ^{-1}) the rate will increase as the temperature rises. The physical picture behind the opposite temperature dependences of the resonant and nonresonant energy transfers is that a faster dephasing leads to a shorter donor/acceptor coherence between the donor and the acceptor, but a larger probability of frequency overlap if the central frequencies of donor and acceptor are off resonance. A shorter coherence leads to a slower resonant energy transfer, but a larger frequency overlap leads to a larger probability of energy transfer from the off-resonant donor to the acceptor. In the phonon compensation mechanism, according to eqs.24&25, the temperature effect reflects on the temperature dependent Boson occupation number. For the down-flowing ($\omega_D > \omega_A$) energy transfer

process, the temperature dependence of energy transfer rate is

$$k_{DA}(T) \propto \frac{1}{\exp(|\Delta E|/k_B T) - 1} + 1$$

which states that a higher temperature leads to a faster

nonresonant energy transfer. Summarizing the above discussions, both mechanisms suggest that the nonresonant energy transfer is faster at a higher temperature, opposite to the resonant energy transfer. The difference between the two mechanisms is that the temperature dependence of the phonon compensation mechanism is a well-defined function if the density of states is temperature independent, but that of the dephasing mechanism is not as quantitative. The temperature dependences of energy transfer rate can be experimentally tested.

3.3.3 The Quantitative Level

Eq.5 can be experimentally quantitatively tested. The energy transfer rate constant (k_{DA}) can be determined by energy transfer experiments through the vibrational energy exchange method or the anisotropy decay method.⁴⁹ The energy gap ($\Delta\omega$) can be determined with FTIR, and the dephasing time can be indirectly determined by the energy gap dependent energy transfer experiments. The remaining parameter, the coupling strength (V), can be determined through the transition dipole/transition dipole interaction⁵⁰

$$V^2 = \frac{1}{n^4} \frac{\mu_D^2 \mu_A^2}{(4\pi\epsilon_0)^2} \frac{\kappa^2}{r_{DA}^6}, \quad \text{eq.26}$$

where n is the refractive index which may need a local field correction factor for some cases⁵⁰. ϵ_0 is the vacuum permittivity. μ_D and μ_A are the transition dipole moments of the donor and acceptor respectively. r_{DA} is the distance between the donor and acceptor.

κ is the orientation factor determined by the relative orientations of the donor and the

acceptor. Eq.26 requires r_{DA} to be larger than the sizes of the donor and acceptor in order to obtain a reasonably precise result⁵¹, which can be fulfilled in many intermolecular vibrational energy transfers between two relatively localized modes, because in these cases r_{DA} is between 2 to 10 angstroms and the sizes of the vibrational modes are 1~2 angstroms which is the length of a typical chemical bond. Combining eqs.5 and 26, one can quantitatively test the validity of eq.5 with samples of well-defined donor/acceptor distances and orientations, or derive the donor/acceptor distances from the vibrational energy transfer measurements.

Different from eq.5, eqs.24&25 are difficult to be experimentally quantitatively evaluated, because the phonon density of states ($\rho_s(\Delta E)$) and the phonon/system coupling ($V_{ph}(s,q)$) are difficult to be experimentally quantitatively determined. Estimates of the general phonon density of states (energy < 200 cm^{-1}) can be experimentally obtained from combinations of far IR (or THz) absorption, Raman, and Neutron scattering experiments, but not all experimentally measured phonons may be involved in the energy transfer process and not all phonons involved are experimentally accessible. Therefore, the effective phonons and their coupling strengths to the energy transfer systems can at most be estimated. To semi-quantitatively address this issue, previous theories suggested that certain types of phonons, e.g. acoustic phonons, participate into the nonresonant electronic energy transfers.^{32, 35}

3.3.4 The Relative Importance

Both mechanisms may simultaneously play roles in nonresonant intermolecular vibrational energy transfers in condensed phases. Which mechanism is more important depends on the detailed situation. We expect that in liquid samples of relatively small

energy gaps (e.g. $\frac{\Delta\omega}{\tau^{-1}} < 10$) where well defined phonons are scarce and vibrational dephasings are generally fast, the energy transfer through the dephasing mechanism can be much faster than that through the phonon compensation mechanism. In crystalline samples with relatively large energy gaps (e.g. $\frac{\Delta\omega}{\tau^{-1}} > 10$), vibrational dephasings are relatively slow, and many phonons with energy equal to the donor/acceptor gap can be available. Under the conditions, the energy transfer through the phonon compensation mechanism can be dominant. In glass, the vibrational dephasing is relatively slow but the phonon density is not as large as that in the crystalline sample, either mechanism can be important.

4. Experimental Results

4.1 Energy Transfer Systems and Methods of Rate Measurements

The energy transfer systems we studied are KSCN/KS¹³CN/KS¹³C¹⁵N crystals and their aqueous and DMF solutions. In the samples, the vibrational energy of the nitrile stretch first excited state can resonantly and nonresonantly transfer among the three anions: SCN⁻, S¹³CN⁻, and S¹³C¹⁵N⁻. In the vibrational energy transfers the energy donor and acceptor are the nitrile stretch modes. In the crystalline samples at room temperature, the CN stretch 0-1 transition frequency of SCN⁻ is 2051 cm⁻¹ with a (fit) Lorentzian line width 5.0 cm⁻¹, and those of S¹³CN⁻ and S¹³C¹⁵N⁻ are 2003 cm⁻¹ and 1976 cm⁻¹ respectively (fig.1A&B). The line widths are the same for all three nitrile stretches. In DMF (fig.1C&D), the frequencies of the three nitrile stretches all blueshift for 6 cm⁻¹ but the gaps between any two remain the same, and the line widths increase to ~7.0 cm⁻¹. In

D₂O (fig.1E&F), the nitrile frequencies blueshift by a larger amount -15 cm⁻¹ again- with the same energy gaps, and the line widths broaden to 14 cm⁻¹.

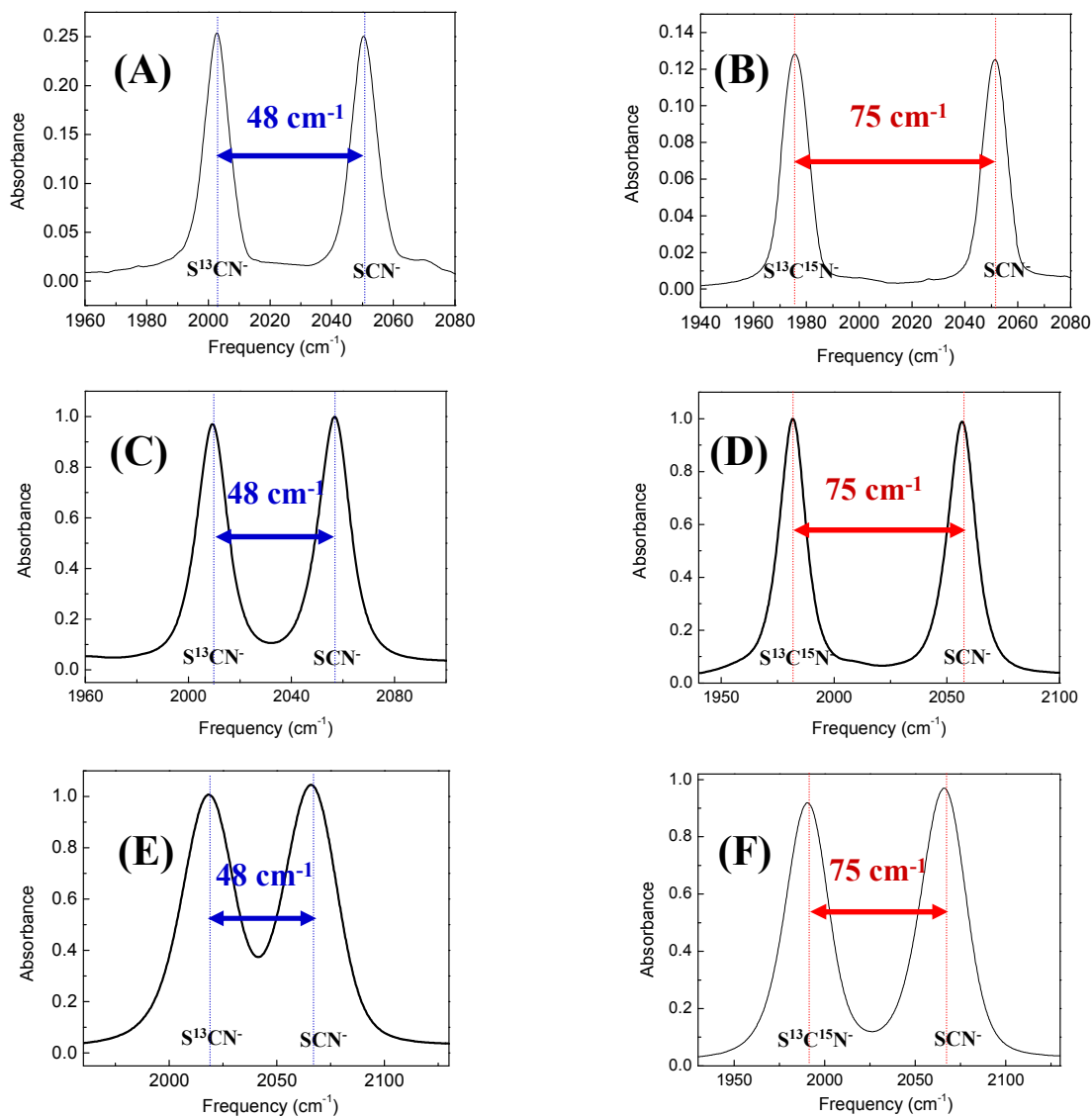


Figure 1. FTIR spectra of $KSCN/KS^{13}CN=1/1$ and $KSCN/KS^{13}C^{15}N=1/1$ showing the nitrile stretch 0-1 transition peaks in (A) and (B) the crystalline samples, in (C) and (D) DMF (with a 1/8 salt/DMF molar ratio, $\sim 1.6M$) saturated solutions, and in (E) and (F) D₂O (10M) saturated solutions at room temperature.

In the three types of samples, the molecular environments are very different as partially indicated by the line width changes, but the energy gaps among the three nitrile stretches remain the same at the values of 48 cm^{-1} (between SCN^- and S^{13}CN^-) and 75 cm^{-1} (between SCN^- and $\text{S}^{13}\text{C}^{15}\text{N}^-$). Because the electronic properties including the nitrile stretch 0-1 transition dipole moments of the three anions are hardly affected by the isotope substitutions, measuring the vibrational energy transfers among them can explicitly reveal the donor/acceptor energy gap dependent energy transfer rates in different environments.

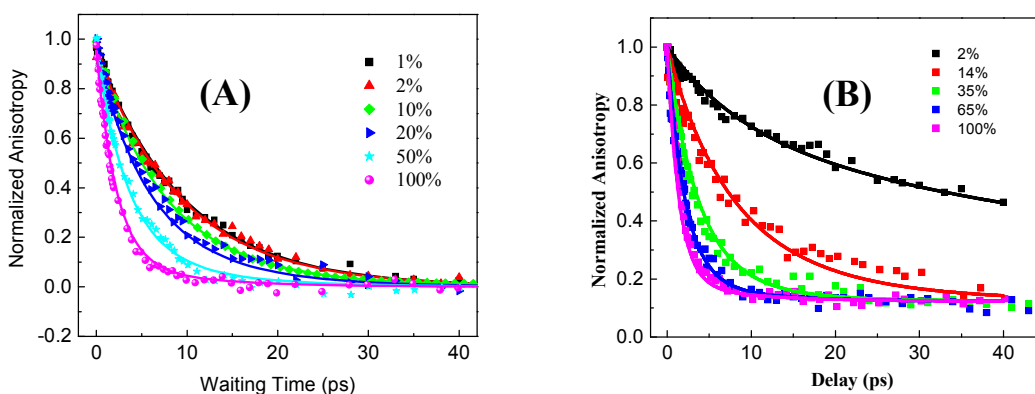


Figure 2. Waiting time dependent anisotropy decays of the nitrile stretch vibrational excitation signal with different resonant energy acceptor ratios (by adjusting the ratio of $\text{KSCN}/\text{KS}^{13}\text{C}^{15}\text{N}$) of (A) $\text{KSCN}/\text{KS}^{13}\text{C}^{15}\text{N}$ D_2O saturated solutions (10M), and (B) $\text{KSCN}/\text{KS}^{13}\text{C}^{15}\text{N}$ mixed crystals at room temperature. Dots are data, and lines are kinetic model calculations.^{19, 40}

To measure the nitrile stretch resonant vibrational energy transfer of which the energy gap $\Delta\omega = 0$, we used the resonant energy transfer induced anisotropy decay method.^{19, 40, 52} As shown in fig.2A (unnormalized data are provided in SI), the signal anisotropy of the nitrile stretch ($^{13}\text{C}^{15}\text{N}$) 1st excited state decays with the increase of

waiting time in saturated KSCN/KSC¹³C¹⁵N D₂O solutions with different KSCN/KSC¹³C¹⁵N ratios.¹⁹ In general, anisotropy decay is caused by two types of molecular dynamics: molecular rotations and resonant energy transfer from one molecule to another molecule with a different orientation. The nonresonant energy transfers between SCN⁻ and S¹³C¹⁵N⁻ are too slow (compared to the anisotropy dynamics) to make any significant contributions to the anisotropy decay.^{19, 40} When very few resonant acceptors are available, e.g. in the 1% or 2% samples, the resonant energy transfer is very slow, and the signal anisotropy decay is mainly caused by the rotations of the anion with a time constant $10 \pm 1 ps$. With more resonant energy acceptors available (larger KS¹³C¹⁵N/KSCN ratios), the decay becomes faster. In the 100% sample, the anisotropy decays with a time constant $2.3 \pm 0.2 ps$. This fast decay is mainly the result of fast resonant energy transfer. From the two values, the resonant energy transfer time in the 100% sample is 3ps ($1/(1/2.3 - 1/10)$). In the 50% sample (KSCN/KS¹³C¹⁵N=1/1), the resonant energy transfer time is 6ps. As shown in fig.2B, the same method was also used to measure the resonant energy transfers of the nitrile stretch in the KSCN/KSC¹³C¹⁵N mixed crystals at room temperature. The resonant energy transfer time constant in the pure crystal is 1.8ps and that in the 1/1 mixed crystal is 3.6ps.⁴⁰ The resonant energy transfers in other samples were measured using the same methods. A difference between the signal anisotropy decays in the liquid and solid samples is that the anisotropy values at long waiting times are zero in the liquid samples but nonzero in the solid samples. The reason is that in liquids the molecular rotations and orientations are completely randomized, but in the solids the rotations are hindered and the relative orientations of the molecules are not random which leads to a residual anisotropy. The residual anisotropy

value was quantitatively calculated based on the hindered rotations and the relative molecular orientations in the crystals.⁴⁰ We also did experiments and verified that that the isotope substations in $S^{13}C^{15}N^-$ have negligible effects on the rotation and resonant energy transfer dynamics as the measured rotational and resonant energy transfer time constants are the same for both SCN^- and $S^{13}C^{15}N^-$ anions.

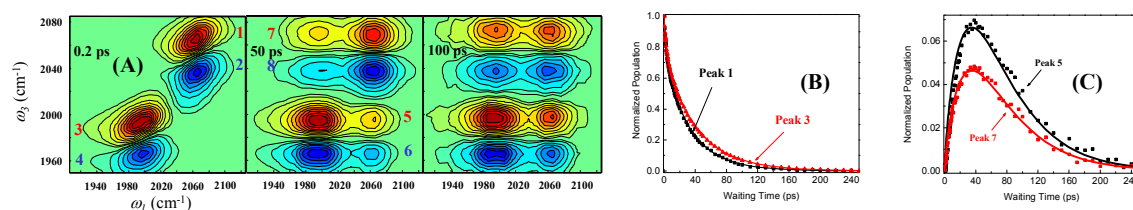


Figure 3. (A) 2D IR spectra of a saturated (10M) $KSCN/KS^{13}C^{15}N=1/1$ D_2O solution at room temperature at three waiting times; (B) and (C) the waiting time dependent intensities of peaks 1, 3, 5, 7 in (A). The parameters in the calculations of (B)&(C) were provided in our previous publication.¹⁹

To measure the nonresonant energy transfers of nitrile stretches between SCN^- and $S^{13}CN^-$ with an energy donor/acceptor gap of 48 cm^{-1} and between SCN^- and $S^{13}C^{15}N^-$ with an energy donor/acceptor gap of 75 cm^{-1} , the vibrational energy exchange method^{18, 19} was used. Fig.3A displays the waiting time dependent 2D IR spectra of a saturated $KSCN/KS^{13}C^{15}N=1/1$ D_2O solution for which the FTIR spectrum is shown in fig.1F. At very short waiting time, e.g. 0.2ps, there are only two pairs of peaks on the diagonal positions in the spectrum. Peaks 1&2 are the CN stretch 0-1 and 1-2 transition peaks respectively, and Peaks 3&4 are the corresponding transition peaks of the $^{13}C^{15}N$ stretch. With the increased waiting time, the vibrational excitations of both nitrile stretches begin to exchange, which produces two pairs of peaks (Peaks 5~8) on the off-diagonal positions (panel 50&100ps). Peaks 5&6 originate from the energy transfer from

the CN stretch 1st excited state to that of the ¹³C¹⁵N stretch, and Peaks 7&8 originate from the reverse energy transfer. From panels 50ps and 100ps, it can be seen that the peak amplitudes of 5&6 are larger than those of 7&8 at the same waiting time. This is because of the detailed balance principle: energy down-flowing must be faster than the up-energy process with a rate ratio determined almost exactly by the Boltzmann factor. Simultaneous analyzing the time dependent intensities of Peaks 1, 3, 5, and 7 with the energy exchange kinetic model quantitatively gives the energy transfer time constants of

both down-flowing ($\frac{1}{k_{CN \rightarrow ^{13}C^{15}N}}$) and up-pumping ($\frac{1}{k_{^{13}C^{15}N \rightarrow CN}}$) processes to be $\frac{1}{k_{CN \rightarrow ^{13}C^{15}N}} = 115 \pm 10 ps$, and $\frac{1}{k_{^{13}C^{15}N \rightarrow CN}} = 164 \pm 15 ps$ (fig.3B&C).¹⁹ Analyzing Peaks 2, 4,

6, and 8 gives the same results.¹⁹ The energy transfer rate ratio $\frac{k_{^{13}C^{15}N \rightarrow CN}}{k_{CN \rightarrow ^{13}C^{15}N}}$ is determined

to be 0.7, which is identical to the Boltzmann factor of the energy difference between the CN and ¹³C¹⁵N stretches ($e^{-\frac{\Delta\omega}{RT}} = e^{-\frac{75}{200}} = 0.7$), verifying the prediction by the detailed balance principle in the energy transfer equations eqs.5&24&25. Using the same method, the energy transfers between the two nitrile stretches in a KSCN/KS¹³C¹⁵N=1/1 mixed crystal at room temperature were also measured. Data are provided in **Section 4.5**.

4.2 Vibrational Energy Transfers in Aqueous Solutions

The nonresonant and resonant vibrational energy transfers among the nitrile stretches in KSCN/KS¹³CN/KS¹³C¹⁵N aqueous solutions of concentrations from 1M to saturation at room temperature were previously measured by us.^{18, 19, 40} Here we use these data to further analyze the energy transfer mechanism and molecular structures behind them. As reported¹⁸ and discussed above, in a saturated KSCN/KS¹³C¹⁵N=1/1 D₂O

solution, the nonresonant energy transfer time from the CN stretch to the $^{13}\text{C}^{15}\text{N}$ stretch with the energy gap $\Delta\omega = 75 \text{ cm}^{-1}$ is $\frac{1}{k_{\text{CN}\rightarrow^{13}\text{C}^{15}\text{N}}} = 115 \pm 15 \text{ ps}$, and the resonant energy

transfer time of the CN stretches with $\Delta\omega = 0 \text{ cm}^{-1}$ is $\frac{1}{k_{^{13}\text{C}^{15}\text{N}\rightarrow^{13}\text{C}^{15}\text{N}}} = \frac{1}{k_{\text{CN}\rightarrow\text{CN}}} = 6 \pm 0.6 \text{ ps}$.

In a saturated $\text{KSCN}/\text{KS}^{13}\text{CN}=1/1$ D_2O solution, the nonresonant energy transfer time from the CN stretch to the ^{13}CN stretch with the energy gap $\Delta\omega = 48 \text{ cm}^{-1}$ is $\frac{1}{k_{\text{CN}\rightarrow^{13}\text{CN}}} = 46 \pm 7 \text{ ps}$. In other words, with the energy gap increase from 0 to 48 cm^{-1} to

75 cm^{-1} , the energy transfer time slows down from 6 ps to 46 ps to 115 ps . This large rate change can be seen by simple inspection of the anisotropy decay curve and the 2D IR spectra in fig.4.

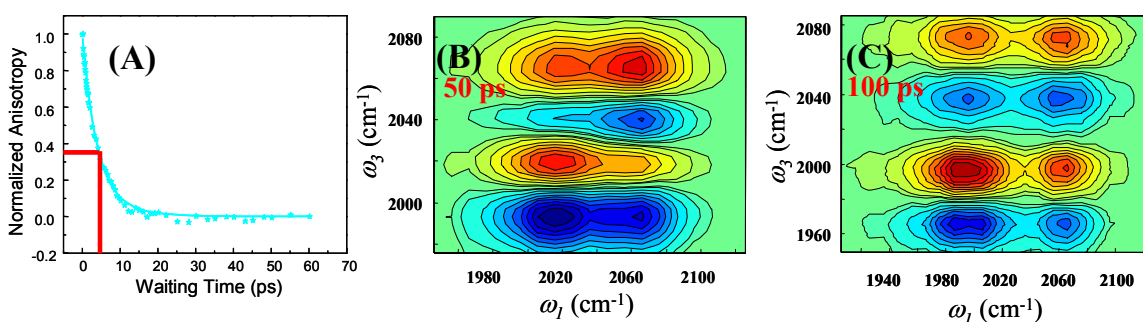


Figure 4. (A) The $^{13}\text{C}^{15}\text{N}$ stretch 1^{st} excited state excitation signal anisotropy decay curve (blue) of a saturated $\text{KSCN}/\text{KS}^{13}\text{C}^{15}\text{N}=1/1$ D_2O solution. The red lines indicate roughly where the decay time constant is. (B) The 2D IR spectrum of a saturated $\text{KSCN}/\text{KS}^{13}\text{CN}=1/1$ D_2O solution at a waiting time 50 ps. The similar intensities of corresponding diagonal and cross peaks along the y-axis indicate that the energy transfer time constant is around 50ps. (C) The 2D IR spectrum of a saturated $\text{KSCN}/\text{KS}^{13}\text{C}^{15}\text{N}=1/1$ D_2O solution at a waiting time 100 ps. The similar intensities of

corresponding diagonal and cross peaks along the y -axis indicate that the energy transfer time constant is around 100ps. The detailed quantitative energy transfer time constants are obtained from rigorous kinetic model calculations.^{18, 19}

The energy transfer slows down for more than twofold when the energy gap increases from 48 cm^{-1} to 75 cm^{-1} . As discussed in Section 3, either the dephasing mechanism or the phonon compensation mechanism can lead to energy gap dependent energy transfer rates. We first consider the phonon compensation mechanism. According to eq.24, in order for the energy transfer rate with a gap 48 cm^{-1} to be 2.5 times of that with a gap 75 cm^{-1} , the effective phonon density ratio at the two energy gaps needs to be

$\frac{\rho_{\text{eff}}(75\text{cm}^{-1})}{\rho_{\text{eff}}(48\text{cm}^{-1})} = 1.7$. However, as discussed above, the effective phonon density involved

in energy transfer cannot be experimentally measured. The relative amplitudes of system/phonon coupling strength $V_{ph}(s, q)$ inside $\rho_{\text{eff}}(\Delta E)$ can only be estimated. The value of $V_{ph}(s, q)$ is mainly determined by the phonon modulation difference between the ground state and the first excited state of which the energy difference is about 2000 cm^{-1} for both from CN to ^{13}CN and from CN to $^{13}\text{C}^{15}\text{N}$ energy transfer processes. Because the chemical properties of these three nitrile stretches are essentially identical and the 1st excited state energy difference between ^{13}CN and $^{13}\text{C}^{15}\text{N}$ is only 27 cm^{-1} which is significantly smaller than the energy gap between the ground and first excited states. Therefore, the system/phonon coupling strengths in both nonresonant energy transfer processes are expected to be very similar if the phonon natures at both energy gaps are similar. We can also estimate the relative amplitudes of phonon density ($\rho_s(\Delta E)$) from far IR (THz) or Raman or Neutron scattering measurements in an approximate way. Fig.5

displays (A) the room temperature THz absorption spectra of a KSCN crystalline sample (300 micron thick), a KSCN/D₂O saturated solution sample (about 0.5~3 micron thick), and a KSCN/DMF saturated solution (0.5~3 micron thick); (B) the room temperature Raman spectra of KSCN/KS¹³C¹⁵N=1/1 and KSCN/KS¹³CN=1/1 crystalline samples; and (C) the Neutron scattering data of crystalline KSCN at 10K in the frequency range of the two energy gaps⁵³. In the D₂O and DMF KSCN solutions, the absorbance from 40 cm⁻¹ to 80 cm⁻¹ slightly increases in a continuous way. These are the absorption of the solvents. In the KSCN crystal, there is an absorption peak at 70~75 cm⁻¹. This peak appears in all the three different types of measurements. If we assume that $\rho_s(\Delta E)$ is proportional to the absorption coefficient which can be obtained from the solution spectra is fig.5A, the calculated energy transfer rate ratio at the two energy gaps (48 and 75 cm⁻¹) based on eq.24 is consistent with the measured rate ratio. However, as measured, the energy transfer rates with the energy gap 75 cm⁻¹ in both D₂O solution and crystal are about the same, and the vibrational couplings in both samples are also very similar.⁴⁰ $\rho_s(\Delta E)$ and therefore the absorption coefficient should be very similar in both samples (based on the assumption) if the energy transfers in both samples are through the phonon compensation mechanism. This is very different from the absorption measurements in fig.5A that the absorption coefficient of KSCN crystal is about 100 times smaller than those of D₂O or DMF in the frequency range. The result suggests that either the assumption that $\rho_s(\Delta E)$ is proportional to the absorption coefficient or the phonon/system coupling is constant is invalid or the energy transfer is not through the phonon compensation mechanism. If the assumption is invalid (our results in solids to be discussed do strongly suggest that there is some strong connection between the optical spectral density and $\rho_s(\Delta E)$), the phonon

compensation mechanism can still be conceivable but another way yet to be developed, is needed to test it. If the phonon compensation mechanism is invalid, the energy transfer can go through the other mechanism – the dephasing mechanism.

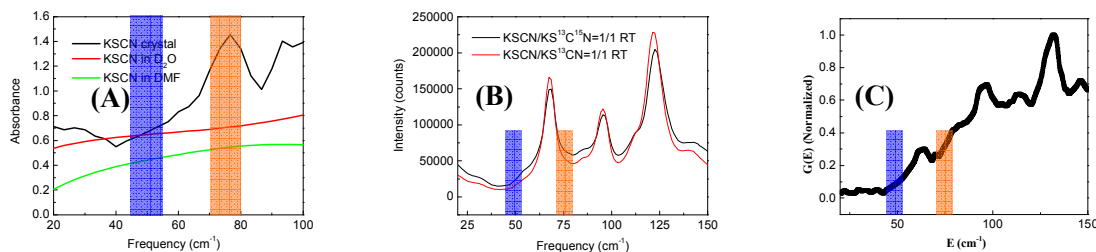


Figure 5. (A) The room temperature THz absorption spectra of a KSCN crystalline sample (300 microns thick), a KSCN/D₂O saturated solution sample (about 0.5~3 microns thick), and a KSCN/DMF saturated solution (0.5~3 microns thick); (B) the room temperature Raman spectra of KSCN/KS¹³C¹⁵N=1/1 and KSCN/KS¹³CN=1/1 crystalline samples. The results show that the isotope labeling doesn't change the phonon modes; and (C) the Neutron scattering data of crystalline KSCN at 10K in the frequency range of 20~100 cm⁻¹. The neutron scattering data are obtained from literature.⁵³ The two semitransparent columns indicate the two energy gaps 48 cm⁻¹ and 75 cm⁻¹.

If the energy transfers are through the dephasing mechanism, eq.5 must be able to describe both the resonant energy transfer and the two nonresonant energy transfers with the same parameters. From experiments (T=295K), we know three energy transfer time constants $1/k = 6, 46, \text{ and } 115\text{ps}$ from energy transfers with three energy gaps $\Delta\omega = 0, 48, \text{ and } 75\text{ cm}^{-1}$. Eq.5 has only two unknown parameters (V and τ), and we have three sets of data which guarantee single values for the two parameters. Substituting the energy transfer rate constants and energy gaps into eq.5, we obtain $V = 4.1\text{ cm}^{-1}$ and $\tau^{-1} = 15\text{ cm}^{-1}$. With these two constants, the calculated energy transfer time constants are

6.1ps ($\Delta\omega = 0$), 49ps ($\Delta\omega = 48 \text{ cm}^{-1}$) and 105ps ($\Delta\omega = 75 \text{ cm}^{-1}$). These values are the same as those experimental results within experimental uncertainty. Here one issue needs to be emphasized. In converting the dephasing time τ with the line width (τ^{-1}) in the denominator of eq.5, a factor of 2π is needed, e.g. if $\tau^{-1} = 15 \text{ cm}^{-1}$, τ must be

$$\tau = \frac{1}{2\pi} \frac{100}{15 \times 3} \text{ ps} = 0.35 \text{ ps}.$$

Now, we need to evaluate whether the two obtained parameters $V = 4.1 \text{ cm}^{-1}$ and $\tau^{-1} = 15 \text{ cm}^{-1}$ are in reasonable ranges. As discussed in Section 3, the energy transfer dephasing line width (τ^{-1}) must not be larger than the sum of the donor and acceptor 0-1 transition line widths. As determined in fig.1E&F, the nitrile stretch line width in the saturated D₂O solution is 14 cm^{-1} . The line width sum of the energy donor and acceptor is therefore 28 cm^{-1} . The determined energy transfer line width $\tau^{-1} = 15 \text{ cm}^{-1}$ is about 50% of the sum, indicating that the dephasings of the donor and acceptor are correlated.

To evaluate the coupling strength $V = 4.1 \text{ cm}^{-1}$, we need to know the structures of the aqueous solutions. As we reported previously with many control experiments, ions in concentrated KSCN aqueous solutions contain a large fraction of ion clusters.^{19-22, 54} The measured energy transfers in the saturated D₂O solutions are the sum of energy transfers from one donor to many acceptors that have various distances away from the donor. In our previous treatment,^{18, 19} we averaged the energy transfer rate over the effective acceptors and based on this averaged rate a number of the effective energy acceptors was obtained, e.g. in the saturated KSCN/KS¹³C¹⁵N=1/1 D₂O solution the effective energy acceptor number is 9. Using 9 as the acceptor number, the coupling strength between one donor and one acceptor can be obtained to be $V_{1 \rightarrow 1} = \frac{V}{\sqrt{9}} = \frac{4.1}{3} = 1.4 \text{ cm}^{-1}$. Now we can

use the transition dipole/transition dipole interaction equation eq.26 to calculate the average donor/acceptor distance based on $V_{1\rightarrow 1} = 1.4 \text{ cm}^{-1}$. We have the parameters from literature¹⁹: $n = 1.5$, $\mu_D = \mu_A = 0.33D$, $\langle \kappa \rangle = \sqrt{2/3}$ (randomized, because the rotation of anion is faster than the energy transfer). The donor/acceptor distance r_{DA} is calculated to be $r_{DA} = 5.1 \text{ \AA}$. This value is larger than the shortest anion distance (4.0 angstroms) in the KSCN crystal but smaller than the nominal anion distance (5.6 angstroms) if ion clustering doesn't occur.⁴⁰ If we assume that the ion packing patterns are somewhat similar in the cluster and crystal, the obtained $r_{DA} = 5.1 \text{ \AA}$ is very reasonable. In the KSCN crystal⁴⁰, surrounding one anion, there are four closest anions at a distance of 4.0 angstroms. The next two anions have distances of 4.8 angstroms, and then two at 5.6 angstroms, and two at 6.2 angstroms. The 17 and 18 anions are at the distance of 6.7 angstroms. The obtained average distance is larger than using the first three acceptors (each type of anions divided by 2 as the sample is KSCN/KS¹³C¹⁵N=1/1) but smaller than when the remaining six are also included. We can use another way to estimate the energy donor/acceptor distance based on $V = 4.1 \text{ cm}^{-1}$. If we assume that the ion packing patterns are somewhat similar in the cluster and crystal, in other words, the number of anions in each layer of anions surrounding any one anion is the same in both cluster and crystal but in the crystal the anions have certain orientations and in the crystal the anions have random orientations, the energy transfer measured in the KSCN/KS¹³C¹⁵N=1/1 aqueous solution is mainly contributed from the transfers of one donor to the two closest anions because $\frac{1}{k_{DA}} \propto r_{DA}^6$. Therefore, for this case the one donor to one acceptor

coupling strength $V_{1\rightarrow 1}$ is $V_{1\rightarrow 1} = \frac{V}{\sqrt{2}} = 2.9 \text{ cm}^{-1}$. This coupling strength gives the donor/acceptor distance 4.0 angstroms, the same as in that in the crystal. However, in the saturated solutions, the ion clusters are large and contain many ions. The energy transfer rate measured is not simply the sum of transfers from one donor to many acceptors, but more like a chain reaction. In other words, the energy may transfer from the donor to an acceptor and from this acceptor to another anion, and so on, similar to those in the KSCN crystal.⁴⁰ Obviously, the above estimated donor/acceptor distances are only approximate.

To more precisely evaluate the coupling strength based on the donor/acceptor distance, what is needed is some ion clusters that contain fewer than five anions. Because in such small clusters the anions can form a structure of four anions surrounding one with a same distance as that in the crystal, the anion distance must be close to the shortest distance 4.0 angstroms in the crystal and no chain transfers need to be considered. This is experimentally achievable. As required by chemical equilibrium, in a more dilute KSCN solution, the ion clusters must become smaller and fewer. This was experimentally observed.¹⁹ We previously determined that in the 1M aqueous solutions, more than 25% of the ions form clusters and on average the clusters contain 3 SCN^- anions.^{19, 40} In the

1M KSCN/ $\text{KS}^{13}\text{C}^{15}\text{N}$ =1/1 solution, the energy transfer times are $\frac{1}{k_{\text{CN}\rightarrow^{13}\text{C}^{15}\text{N}}} = 180 \pm 20 \text{ ps}$

($\Delta\omega = 75 \text{ cm}^{-1}$), and $\frac{1}{k_{^{13}\text{C}^{15}\text{N}\rightarrow^{13}\text{C}^{15}\text{N}}} = \frac{1}{k_{\text{CN}\rightarrow\text{CN}}} = 10 \pm 1 \text{ ps}$ ($\Delta\omega = 0$).⁴⁰ Substituting these

values into eq.5, we obtain $V = 3.1 \text{ cm}^{-1}$ and $\tau^{-1} = 15.5 \text{ cm}^{-1}$. The one donor to one

acceptor coupling strength is therefore $V_{1\rightarrow 1} = \frac{3.1}{\sqrt{1.5}} = 2.5 \text{ cm}^{-1}$. Based on the coupling

strength and eq.24 and the above parameters, the donor/acceptor distance r_{DA} in the cluster containing three anions is determined to be 4.3 angstroms, close to the closest anion distance 4.0 angstroms in the crystal. Including all experimental uncertainties of each parameter, we estimate the uncertainty of the determined distance is about 10%~20%. The results indicate that eq.5 of the dephasing mechanism describes the vibrational energy transfers of the KSCN/KS¹³CN/KS¹³C¹⁵N aqueous solutions very well.

The above discussion also resolves an issue that puzzled us for the last two years. We previously observed that on average one-donor-to-one-acceptor resonant energy transfer is faster in a more dilute KSCN aqueous solution, and we speculated that it was because the ions were closer in a smaller cluster.¹⁹ Here we use the previous energy transfer results and eq.5 to derive the average donor/acceptor distances in the ion clusters of the KSCN aqueous solutions of different concentrations. The results are listed in table 1. As we can see from table 1, the energy donor/acceptor average distance is largest (5.1 Å) in the saturated solution (10M). It gradually becomes smaller with the decrease of ion concentration in the solutions. In the 1M solution, the distance is 4.3 Å, very close to that of the shortest distance in the KSCN crystal. We believe that the donor/acceptor distance change doesn't reflect the ion distance change in the ion clusters. Instead, the distance change is more because in the more concentrated solutions, the ion clusters have more ions so that the energy acceptors have to distribute around the energy donor with different distances. The measured energy transfer is the sum of transfers from the donor to all acceptors and the chain transfers from the initial acceptors to the secondary and tertiary acceptors and so on. The result of the chain transfer is that the average donor/acceptor distance is larger than the shortest anion/anion distance. Only in dilute solutions, the ion

clusters are sufficiently small so that all energy acceptors can have a same distance to the donor as constrained by space available. In such solutions, the average donor/acceptor distance is the same as the anion distance in the cluster. Imagining that the crystalline structure applies, surrounding an SCN^- anion, the first solvation shell of a distance 4 Å can contain four SCN^- anions. We expect that in the ion clusters the first solvation of any anion can also contain at most four anions. Because of this restriction, in the 1M and 1.8M solutions where the ion clusters contain 3 and 4 anions the energy donor/acceptor distances are very close to 4 Å. The determined distance 4.3 Å also suggests that the ion clusters are direct contact clusters.

Table 1. *The energy donor/acceptor distances in $\text{KSCN}/\text{KS}^{13}\text{C}^{15}\text{N}$ D_2O solutions with different concentrations determined by the measured energy transfer rates and the number of ions in a cluster and eq.5. Other parameters in the calculations are $n=1.5$, $\mu_D = \mu_A = 0.33D$, $\langle \kappa \rangle = \sqrt{2/3}$.*

	10M	8.8M	6.5M	4M	1.8M	1M
$\frac{1}{k_{\text{CN} \rightarrow \text{CN}}} \text{ (ps)}$	6.0	6.2	7.1	10	9	10
$\frac{1}{k_{\text{CN} \rightarrow ^{13}\text{C}^{15}\text{N}}} \text{ (ps)}$	115	110	130	140	160	180
n (# of anions in cluster)	18	13	9	5	4	3
$\tau^{-1} \text{ (cm}^{-1}\text{)}$	15.0	15.0	15.0	18.0	15.5	15.5
$V_{1 \rightarrow 1} \text{ (cm}^{-1}\text{)}$	1.4	1.57	1.74	2.06	2.34	2.53
$r_{\text{DA}} \text{ (Å)}$	5.1	5.0	4.8	4.6	4.4	4.3

In summary, eq.5 of the dephasing mechanism and the transition dipole/transition dipole interaction eq.26 quantitatively describe both resonant and nonresonant vibrational energy transfers in the KSCN/KS¹³CN/KS¹³C¹⁵N D₂O solutions very well. However, the anion distances in the ion clusters are difficult to determine by other experimental techniques. A system with a well-defined donor/acceptor distance that can be determined by some mature techniques, e.g. XRD, is highly desired to benchmark the method. We recently made a significant step towards this goal by directly measuring the resonant energy transfers among the SCN⁻ anions in KSCN crystal. Using eqs.5&26, the shortest anion distance determined from the experimental energy transfer time constant is $3.9 \pm 0.3 \text{ \AA}$, identical to that (4 \AA) determined by XRD.⁴⁰

4.3 Temperature Dependent Vibrational Energy Transfers in Aqueous Solutions

One of the interesting predictions of eq.5 is that the resonant energy transfer will become slower and the nonresonant energy transfer will become faster at a higher temperature if $\Delta\omega > \tau^{-1} > V$ (for $\Delta\omega \neq 0$) and $\tau^{-1} > V$ (for $\Delta\omega = 0$) and no chemical transformations occur within the temperature range, because at a higher temperature molecular motions are faster and the energy transfer dephasing caused by the motions typically becomes faster accordingly (τ^{-1} is larger at a higher temperature). The faster energy transfer dephasing may be because of faster donor/acceptor dephasings and/or because the dephasings of donor and acceptor are less correlated. Measurements on the resonant and nonresonant vibrational energy transfers in the KSCN/KS¹³C¹⁵N D₂O 10M solutions from room temperature to 80⁰C fulfill the requirements. As described above, at room temperature, the resonant energy transfer among the nitrile stretch in the

KSCN/KS¹³C¹⁵N=1/1 D₂O 10M solutions has a time constant 6ps, and the nonresonant energy transfer from SCN⁻ to S¹³C¹⁵N⁻ with an energy gap 75 cm⁻¹ has a time constant 115ps. As shown in fig.6, at 80⁰C, the resonant energy transfer time slows down to 6.8ps ($2 / (\frac{1}{1.7} - \frac{1}{3.4}) = 6.8$) from 6ps at room temperature, but that of the nonresonant energy transfer becomes faster to 95ps from 115ps. The observed opposite temperature dependences of resonant and nonresonant energy transfers are consistent with the prediction by eq.5. Substituting the two values into eq.5, we obtain $V = 4.1 \text{ cm}^{-1}$ and $\tau^{-1} = 17.5 \text{ cm}^{-1}$ with calculated resonant transfer time 6.7ps and the nonresonant time 94ps at 80⁰C. The coupling strength is the same as that (4.1 cm⁻¹) at room temperature, but the dephasing line width is larger than that (15 cm⁻¹) at room temperature. The same coupling strength indicates that the average anion distance at 80⁰C is similar to that at room temperature in the same solution, because the other parameters in equation eq.26 which correlate the coupling strength to the distance are weakly temperature dependent. This is consistent with the temperature dependent FTIR measurements (in SI). The larger energy transfer dephasing line width indicates that the energy transfer dephasing at 80⁰C is faster. As discussed, this is probably because the molecular motions are faster. This is supported by the faster molecular rotation at 80⁰C (3.4ps) compared to that (10ps) at room temperature.

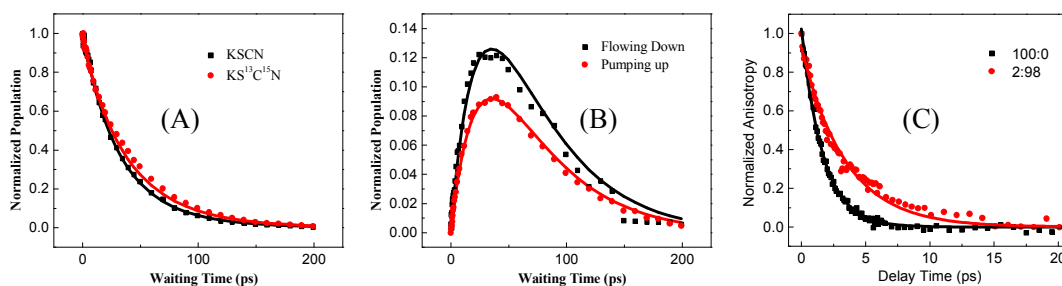


Figure 6. (A)&(B) are the intensities of 1-2 transition peaks (similar to peaks 2, 4, 6, 8 in fig.3) of 10M KSCN/KS¹³C¹⁵N=1/1 D₂O solutions at 80⁰C. Dots are data and curves are kinetic model calculations. (C) Anisotropy decays of the nitrile stretch first excited state with 2% resonant energy acceptor (red) and with 100% resonant acceptor in 10M KSCN/KS¹³C¹⁵N D₂O solutions at 80⁰C. Dots are data and curves are fits with single exponentials with time constant 3.4ps (red) and 1.7ps (black).

4.4 Resonant and Nonresonant Energy Transfers in DMF Solutions

The energy-gap dependence of vibrational energy transfers in the D₂O solutions described above is also observed in KSCN/KS¹³CN/KS¹³C¹⁵N DMF solutions with a salt/DMF ratio 1/8, though the molecular properties and intermolecular interactions in the D₂O and DMF solutions are very different.

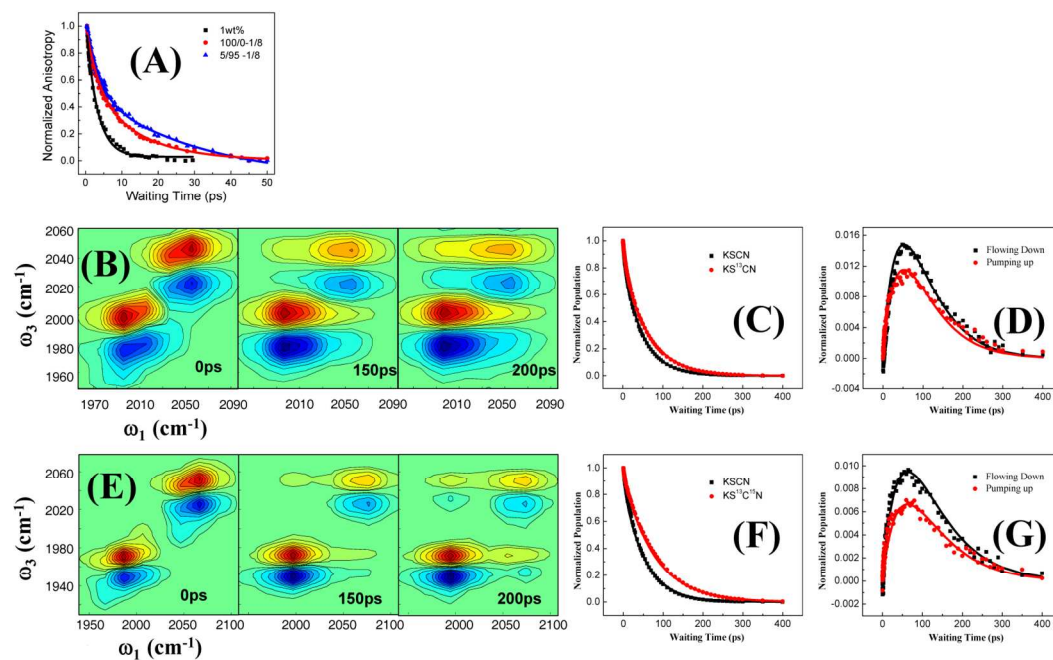


Figure 7. (A) Anisotropy decay data of CN stretch 1st excited state of 1wt% KSCN in DMF (black), a KSCN/DMF solution with a 1/8 molar ratio (~1.6M), and of ¹³C¹⁵N stretch 1st excited state of a KS¹³C¹⁵N/KSCN = 5/95 DMF solution with a 1/8 salt/DMF

molar ratio. Dots are data, and lines are single exponential fit (black) with and biexponential fits (red&blue).¹⁷ (B) Waiting time dependent 2D IR spectra of a KSCN/KS¹³CN = 1/1 DMF solution with a 1/8 salt molar ratio (~1.6M). (C)&(D) The time dependent diagonal and cross blue peak intensities of (B). Dots data and curves are kinetic model calculations. (E) Waiting time dependent 2D IR spectra of a KSCN/KS¹³C¹⁵N = 1/1 DMF solution with a 1/8 salt molar ratio. (F)&(G) The time dependent diagonal and cross blue peak intensities of (E). Dots are data and curves are kinetic model calculations.

We also used the anisotropy decay method to measure the resonant energy transfer rate among the SCN⁻ anions in the 1/8 KSCN/DMF solution. As displayed in fig.7A, different from that in the D₂O solutions, the anisotropy decays of the CN stretch of the pure KSCN and the ¹³C¹⁵N stretch of the 5/95 sample in the 1/8 solutions are not single exponential. They exhibit a clear biexponential behavior: a fast component with a weighing factor ~44% and a time constant 3.4ps and a slow component with a weighing factor 56% with a time constant 13.7ps (100% KSCN solution) and 30.7ps (KS¹³C¹⁵N/KSCN = 5/95) respectively. In a very dilute (1wt%) KSCN DMF solution, the anisotropy decay of CN excitation is a single exponential with a time constant 3.1ps (black in fig.7A), which is the rotational time constant of the free anions as in such a dilute solution most ions are expected to be separated by the DMF solvent molecules. Similar to the D₂O solutions, KSCN ions in the concentrated 1/8 DMF solutions are expected to form some ion clusters. We suspect that the fast decay component of the 1/8 samples is because of the rotation of the free anions in the solutions, as the time constant (3.4ps) is very similar to that (3.1ps) of the free anion in the dilute solution, and the slow

component is because of the rotation and the resonant energy transfer of the ion clusters. With such an assumption, the ion cluster ratio in the 1/8 solutions is the weighing factor of the slow component, 56%. The number of the anions in the cluster can be estimated to be around 4~6 from the rotational time ratio between the clustered and free anions ($30.7/3.4 \sim 9$) and the estimated relative volume ratio of the anion/cation. More discussion on the analysis is provided in SI. The resonant energy transfer time in the pure KSCN 1/8 solution can be obtained from the rate difference between the 100% and 5/95 1/8 samples ($1/(1/13.7-1/30.7)$) to be 24.7ps, which indicates that the resonant energy transfer time constant in the KSCN/KS¹³C¹⁵N=1/1 1/8 DMF solution would be $24.7*2=49.4$ ps as the number of acceptors is 50% fewer. Based on the cluster ratio 56% and 2D IR energy exchange measurements (fig.7B~G), the vibrational energy transfer time constant from CN to ¹³CN in a KSCN/KS¹³CN=1/1 1/8 DMF solution is determined to be 570ps, and that from CN to ¹³C¹⁵N in a KSCN/KS¹³C¹⁵N=1/1 1/8 DMF solution is determined to be 1150ps. Substituting the three time constants 49.4ps ($\Delta\omega = 0$), 570ps ($\Delta\omega = 48 \text{ cm}^{-1}$) and 1150ps ($\Delta\omega = 75 \text{ cm}^{-1}$) into eq.5, we obtain the coupling strength $V = 1.25 \text{ cm}^{-1}$ and the dephasing width $\tau^{-1} = 14 \text{ cm}^{-1}$ with the calculated time constants 49ps ($\Delta\omega = 0$), 542ps ($\Delta\omega = 48 \text{ cm}^{-1}$) and 1191ps ($\Delta\omega = 75 \text{ cm}^{-1}$). The dephasing width is the sum of the donor/acceptor 0-1 transition line widths. Based on $V = 1.25 \text{ cm}^{-1}$ and the estimated anion number in the cluster (4~6) and eq.26, the distance between two anions in an ion cluster in the 1/8 DMF solutions is 5.3Å (the transition dipole moment in DMF is about 27% smaller than that in D₂O). This value is about 20% larger than the shortest anion distance 4.0 Å in the KSCN crystal but significantly smaller than the average anion distance ~1nm in the DMF solution if ions didn't form clusters. The

analysis shows that the vibrational energy transfers in the DMF solutions with three different donor/acceptor energy gaps can be simultaneously described by eq.5 reasonably well.

Summarizing the results in the KSCN/KS¹³CN/KS¹³C¹⁵N D₂O and DMF solutions, we conclude that eq.5 of the dephasing mechanism and eq.26 of the transition dipole/transition dipole interaction describe the intermolecular vibrational energy kinetics and the correlation between the donor/acceptor distance and coupling in the solution very well. However, the experimental results don't provide strong evidence to support or object to eqs.24&25 of the phonon compensation mechanism of the second order perturbation approach, though comparing the results in the D₂O and DMF solutions could provide some indirect hint again the phonon compensation mechanism. D₂O and DMF are very different molecules. One would expect that the phonon densities (though the THz absorption patterns in the range of 30~100 cm⁻¹ are similar in fig.5A) and the phonon/anion interactions in the two solutions should be very different. If eqs24&25 work, the energy donor/acceptor gap dependences of energy transfers in the two solutions are expected to be very different. This prediction is different from the experimentally observed similar gap dependence. The results seem to provide some evidence that is not easy to explain by the previous phonon compensation mechanism based on the first order perturbation¹⁵: in both samples, the energy transfer rate is about inversely proportional to the square of the energy gap. In order to explain such an observation, the previous theory needs to assume the product of the phonon/system coupling and the phonon density at 48 cm⁻¹ is about 1.5 times of that at 75 cm⁻¹ at room temperature which seems not to be supported by the estimations in literature^{4, 15}.

4.5 Vibrational Energy Transfers in Crystals at Room Temperature

The benchmarking test of eqs.5&26 comes from the resonant energy transfer measurements (fig.2B) in KSCN/KS¹³C¹⁵N crystals of which the energy donor/acceptor (anions) distances⁴⁰ have been well characterized with XRD and Neutron diffraction methods^{53, 55}. The closest anion distance in the KSCN crystal is determined to be $3.9 \pm 0.3 \text{ \AA}$ from the measured resonant energy transfer time constant and eqs.5&26. This value is the same as 4.0 \AA that is determined by XRD. However, the nonresonant energy transfer results in the crystals are very surprising. They don't follow the observed energy gap dependence in the liquid samples described above. As shown in fig.8A&D, the vibrational energy exchange cross peaks of the KSCN/KS¹³CN=1/1 crystalline sample (fig.8A) is only slightly larger than those of the KSCN/KS¹³C¹⁵N=1/1 crystalline sample at the same waiting times at room temperature. The results indicate that the vibrational energy transfer from CN to ¹³CN is only slightly faster than that from CN to ¹³C¹⁵N. Quantitative analyses in fig.8B, C, E, &F show that the energy transfer time from CN to ¹³CN with an energy gap 48 cm^{-1} is $\frac{1}{k_{CN \rightarrow ^{13}CN}} = 96 \pm 5 \text{ ps}$, and that from CN to ¹³C¹⁵N with a gap 75 cm^{-1} is $\frac{1}{k_{CN \rightarrow ^{13}C^{15}N}} = 99 \pm 5 \text{ ps}$. This observed energy gap independence cannot be explained with eq.5 of the dephasing mechanism.

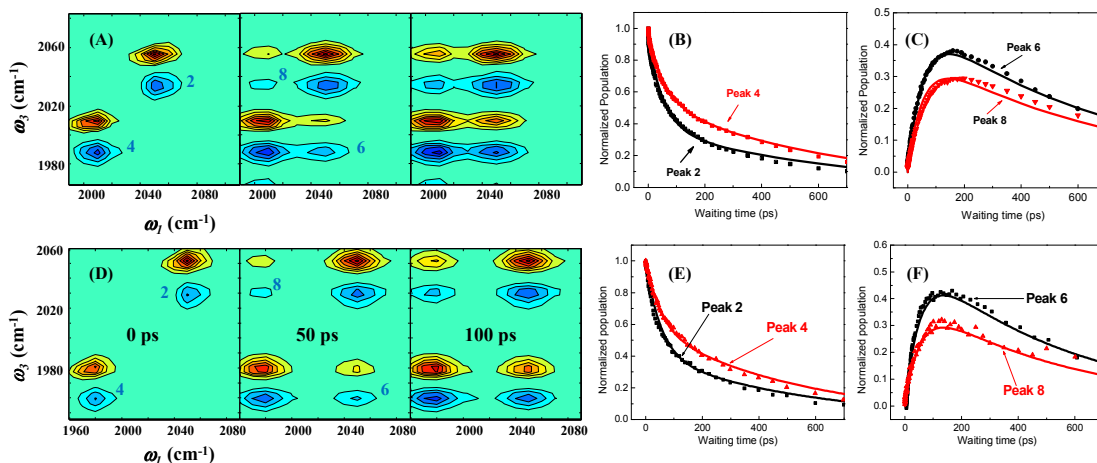


Figure 8. (A) 2D IR spectra of a KSCN/KS¹³CN=1/1 mixed crystal at room temperature at three waiting times; (B) and (C) the waiting time dependent intensities of peaks 2, 4, 6, 8 in (A). Dots are experimental results, and lines are kinetic model calculations. (D) 2D IR spectra of a KSCN/KS¹³C¹⁵N=1/1 mixed crystal at room temperature at three waiting times; (E) and (F) the waiting time dependent intensities of peaks 2, 4, 6, 8 in (D).

As discussed in Section 3, both the dephasing mechanism and the phonon compensation mechanism play roles in nonresonant energy transfers, and depending on the detailed situation, one mechanism may dominate over the other. The nonresonant energy transfer data in fig.8 seem to suggest that the phonon compensation mechanism is dominant in the crystalline samples. To further explore this issue, we first use eq.5 to estimate how fast the nonresonant energy transfers of the dephasing mechanism can be in the two crystalline samples. According to the resonant energy transfer time 3.6ps and the average coupling strength 3.5 cm⁻¹ in the 1/1 mixed crystalline samples and eq.5 (the resonant energy transfer rate needs to be calculated for each donor/acceptor pair⁴⁰), the energy transfer dephasing line width (τ^{-1}) is determined to be 8 cm⁻¹.⁴⁰ Based on the two parameters and eq.5, the energy transfer time for an energy gap 48 cm⁻¹ is calculated to

be $\frac{1}{k_{CN \rightarrow ^{13}CN}} = 117 ps$ and that for an energy gap 75 cm^{-1} is calculated to be

$\frac{1}{k_{CN \rightarrow ^{13}C^{15}N}} = 262 ps$. However, we notice that in the KSCN crystals, the energy transfer

dephasing width 8 cm^{-1} is close to two times (4.6 cm^{-1}) the largest coupling between two adjacent anions. Under such a situation, eq.5 is not very sensitive to τ^{-1} for the resonant energy transfer. τ^{-1} can vary from 3 cm^{-1} to 8 cm^{-1} . This suggests that the actual energy transfer times predicted by eq.5 can be even longer than these two values. Therefore, the

two calculated values suggest that the experimentally observed $\frac{1}{k_{CN \rightarrow ^{13}C^{15}N}} = 99 ps$ must

be mainly from the phonon compensation mechanism, and the experimental

$\frac{1}{k_{CN \rightarrow ^{13}CN}} = 96 ps$ can be dominated by either mechanism depending on the energy

transfer dephasing time. If the dephasing mechanism is not considered, the observed energy gap independence can be qualitatively explained with eq.24&25. If the phonon/system coupling strengths are the same at two energy gaps as discussed above,

and the phonon density at 75 cm^{-1} should be $\left(\frac{75}{48}\right)^2 \times \frac{[\exp(48/200) - 1]^{-1} + 1}{[\exp(75/200) - 1]^{-1} + 1} = 3.6$ times

of that at 48 cm^{-1} , the experimental observations can be predicted by eq.24. It is very interesting to see that all THz absorption, Raman and Neutron scattering measurements (fig.5) do show that the peak density at $\sim 75 \text{ cm}^{-1}$ is at least two times larger than that at 48 cm^{-1} . In the THz absorption spectrum, the peak ratio is about 2.2 times. In the Raman spectrum, the ratio is ~ 7.3 times. The neutron scattering experiments also show that the optical phonon densities at 75 cm^{-1} is significantly larger than those at 48 cm^{-1} (the ratio

is estimated to be more than 5 from literature).⁵⁶ The results seem to suggest that if optical phonons are the major phonons participating in the energy transfer process, the phonon densities at 75 cm^{-1} must be at least a few times larger than those at 48 cm^{-1} . Another possible explanation for the two observed similar nonresonant energy transfer times is that the energy transfers must be energy gap independent if acoustic phonons with Debye approximation are assumed.³² However, this later explanation is not supported by our temperature dependent experiments to be described in later paragraphs. The observed energy gap independence could also be explained by the phonon compensation mechanism of the first order approach if the product of the system/phonon coupling strengths and the phonon densities at 75 cm^{-1} is 1.5 times of that at 48 cm^{-1} . However, if the phonons involved in the transfer are optical phonons, the condition is not fulfilled as the density ratio is much more than 1.5 times as discussed above. If the phonons are acoustic phonons, only the second order perturbation approach will lead to the gap independence. Therefore, we consider that the 1st order perturbation approach¹⁵ is less likely a reason for the observed energy gap independence.

4.6 Temperature dependent Vibrational Energy Transfers in Crystals

4.6.1 Energy Transfers in $\text{KS}^{13}\text{C}^{15}\text{N}/\text{KSCN}=1/1$ Mixed Crystal

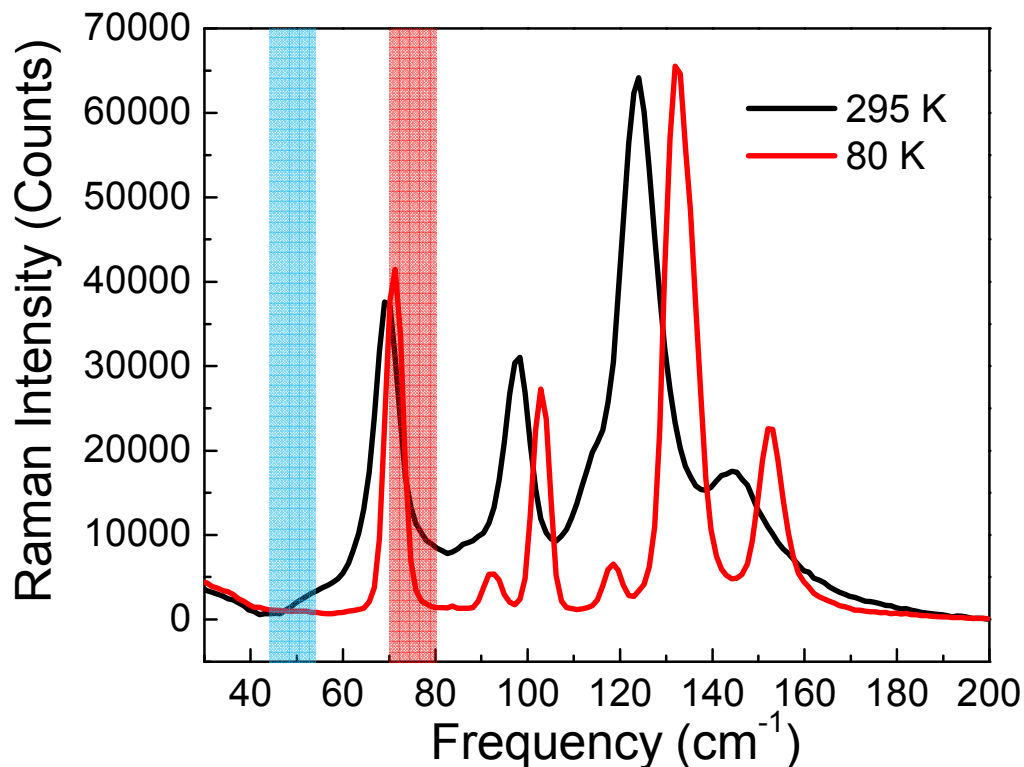


Figure 9. Raman spectra of KSCN crystal at 295K and 80K. The two columns indicate the two energy gaps.

As discussed above, the experimentally observed nonresonant energy transfer from CN to $^{13}\text{C}^{15}\text{N}$ in the $\text{KS}^{13}\text{C}^{15}\text{N}/\text{KSCN}=1/1$ mixed crystal must be mainly determined by the phonon compensation mechanism. This argument can be tested with temperature dependent experiments. According to eq.24, if the conclusion is valid, the energy transfer rate constant $k_{\text{CN} \rightarrow ^{13}\text{C}^{15}\text{N}}$ from CN to $^{13}\text{C}^{15}\text{N}$ must be proportional to $[\exp(|\Delta E|/k_B T) - 1]^{-1} + 1$ where $\Delta E = 75 \text{ cm}^{-1}$, provided that there are no coupling or phonon mode changes. Temperature dependent neutron diffraction studies show that in KSCN crystal no phase transitions occur between 80 K to 295 K, but the unit cell volume

shrinks at a lower temperature with a volume ratio 1.04/1.01/1 (295K/150K/80K).⁵⁷ According to eqs.5&24&26, the volume change leads to a small energy transfer rate change with a ratio 1.08/1.02/1 (295K/150K/80K). Raman scattering measurements in fig.9 shows that the phonon modes around 70~75 cm⁻¹ exist at both room temperature and 80K, with the line width becomes a little narrower and the center frequency slightly blueshifts. Such small frequency changes are expected not to affect the energy transfer rate from CN to ¹³C¹⁵N very much as the FWHM of the nitrile stretch peak is 10 cm⁻¹. Therefore, we expect that the temperature dependence of the energy transfer from CN to ¹³C¹⁵N should follow $[\exp(|\Delta E|/k_B T) - 1]^{-1} + 1$ reasonably well from 80K to 295K. The situation for the energy transfer from CN to ¹³CN is very different. At about 50 cm⁻¹, the absorption peak which is probably the shoulder of the major peak ~70 cm⁻¹ almost completely disappears at 80K. If the phonon densities involved in the energy transfer process are correlated to spectral intensities observed in fig.9, we expect that the energy transfer from CN to ¹³CN at 80K compared to that at 295K must be much slower than that predicted by $[\exp(|\Delta E|/k_B T) - 1]^{-1} + 1$.

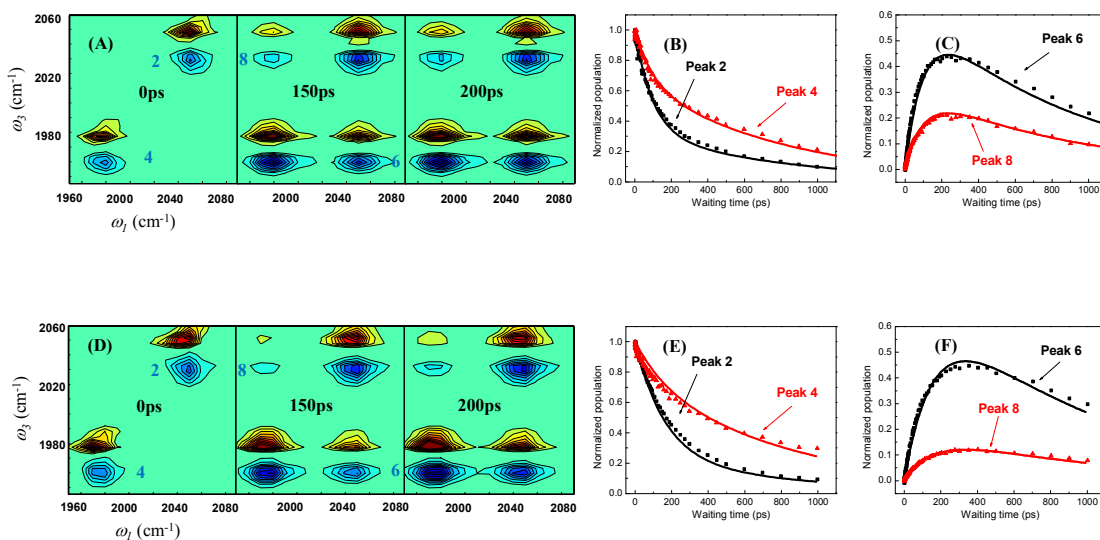


Figure 10. (A) 2D IR spectra of a KSCN/KS¹³C¹⁵N=1/1 mixed crystal at 150K at three waiting times; (B) and (C) the waiting time dependent intensities of peaks 2, 4, 6, 8 in (A). Dots are experimental results, and lines are kinetic model calculations. (D) 2D IR spectra of a KSCN/KS¹³C¹⁵N=1/1 mixed crystal at 80K at three waiting times; (E) and (F) the waiting time dependent intensities of peaks 2, 4, 6, 8 in (D). Dots are experimental results, and lines are kinetic model calculations.

Vibrational energy exchange measurements (fig.10) show that the energy transfer

time from CN to ¹³C¹⁵N is $\frac{1}{k_{CN \rightarrow ^{13}C^{15}N}} = 163 ps$ at 150K and $\frac{1}{k_{CN \rightarrow ^{13}C^{15}N}} = 237 ps$ at 80K.

Combining $\frac{1}{k_{CN \rightarrow ^{13}C^{15}N}} = 99 ps$ at 295K, the experimentally measured energy transfer rate

ratio at the three temperature is 1/1.45/2.37 (80K/150K/295K). The predicted rate ratio

by $[\exp(|\Delta E|/k_B T) - 1]^{-1} + 1$ with the CN/¹³C¹⁵N gap $\Delta E = 75 cm^{-1}$ is 1/1.43/2.38

(80K/150K/295K). Within experimental uncertainty (~5%), the experimental temperature

dependence is identical to the predicted one. Combined with the discussion in Section 4.5,

the results strongly support that the experimentally observed energy transfer from CN to

$^{13}\text{C}^{15}\text{N}$ in the $\text{KS}^{13}\text{C}^{15}\text{N}/\text{KSCN}=1/1$ mixed crystal is mainly determined by the phonon compensation mechanism. This temperature dependence also suggests that the phonon compensation process involves only one-phonon as processes with more phonons have different temperature dependences.^{32,35} For example, if the process involves two phonons at 35 cm^{-1} and 40 cm^{-1} , the temperature dependent energy transfer rate ratio would be 8.7/1 (295K/80K). This is very different from the prediction of one-phonon process 2.38/1 which is identical to the experimental value.

4.6.2 Energy Transfers in $\text{KS}^{13}\text{CN}/\text{KSCN}=1/1$ Mixed Crystal

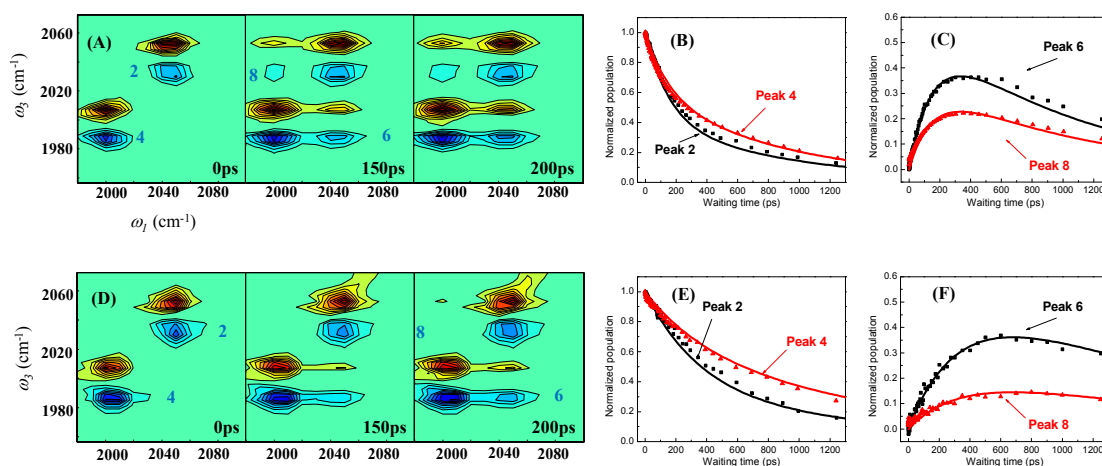


Figure 11. (A) 2D IR spectra of a $\text{KSCN}/\text{KS}^{13}\text{CN}=1/1$ mixed crystal at 150K at three waiting times; (B) and (C) the waiting time dependent intensities of peaks 2, 4, 6, 8 in (A). Dots are experimental results, and lines are kinetic model calculations. (D) 2D IR spectra of a $\text{KSCN}/\text{KS}^{13}\text{CN}=1/1$ mixed crystal at 80K at three waiting times; (E) and (F) the waiting time dependent intensities of peaks 2, 4, 6, 8 in (D). Dots are experimental results, and lines are kinetic model calculations.

As discussed in Section 4.5, if the acoustic phonon with the Debye approximation is assumed, the energy transfer rate would be energy donor/acceptor gap independent. At

room temperature, the observed energy transfers with gaps 48 cm^{-1} and 75 cm^{-1} are very similar. However, at lower temperatures e.g. 150K and 80K, the energy transfer times at these two gaps are very different. The results cannot be explained by the acoustic phonon assumption. As measured (in fig.11A~C), the energy transfer time from CN to ^{13}CN at 150K is $\frac{1}{k_{\text{CN} \rightarrow ^{13}\text{CN}}} = 296 \text{ ps}$, substantially longer than that (163ps) from CN to $^{13}\text{C}^{15}\text{N}$ at the same temperature. At 80K, the difference is even larger. The energy transfer time from CN to ^{13}CN is $\frac{1}{k_{\text{CN} \rightarrow ^{13}\text{CN}}} = 636 \text{ ps}$, about three times of that (237ps) from CN to $^{13}\text{C}^{15}\text{N}$. Now the energy transfer is faster with a larger gap, opposite to those in the liquids discussed above. If we use the energy transfer time $\frac{1}{k_{\text{CN} \rightarrow ^{13}\text{CN}}} = 96 \text{ ps}$ at 300K as the starting point to estimate the time at 80K using $[\exp(|\Delta E|/k_B T) - 1]^{-1} + 1$, the energy transfer time at 80K would be $\frac{1}{k_{\text{CN} \rightarrow ^{13}\text{CN}}} = 259 \text{ ps}$. The predicted value is more than two times faster than that (636ps) experimentally observed. The Raman spectra in fig.9 provide a very likely explanation for this result. At room temperature, the phonon to compensate the energy gap 48 cm^{-1} between CN and ^{13}CN is provided by the shoulder of the phonon (probably optical phonons) modes of $\sim 70 \text{ cm}^{-1}$. At 80K, because the central frequency of the phonon modes blueshifts and the peak becomes narrower, the shoulder of the phonon modes is very small at 48 cm^{-1} so that the phonon density to compensate the energy gap is small and the energy transfer accordingly slows down. Here we want to point out that the discussion is based on the assumption that the phonon density involved in the energy transfer is correlated to the observed Raman intensity. The assumption does

not necessarily reflect the truth as the assumed phonon density change (change for ~6 times from RT to 80K) is much larger than that of the structural change (4% volume change from RT to 80K).

There can be an alternative explanation for the slow energy transfers from CN to ^{13}CN at low temperatures: the dephasing mechanism. If the energy transfer is determined by the dephasing mechanism, the energy transfer dephasing time τ needs to slow down for about 3 times from room temperature to 150K and 6.4 times to 80K. However, such huge dephasing time changes are not easy to imagine as no phase transformations or significant structural changes occur in the temperature range, especially compared to the 17% change of dephasing time in the aqueous solution from room temperature to 80°C described above.

Neither explanation is completely satisfactory. The phonon density loss at 48 cm^{-1} at low temperatures is probably a very important reason for the observed slow energy transfers at low temperatures, but the dephasing mechanism also plays a significant role as the estimated transfer rate at RT based on eq.5 is about 30%~80% of the measured rate. In principle, this issue can be further tested with temperature dependent resonant energy transfer measurements (fig.S2 in SI). However, based on eq.5, in order for

$\frac{1}{k_{\text{CN} \rightarrow ^{13}\text{CN}}} = 296\text{ ps}$ (150K) and 636 ps (80K), the energy transfer dephasing width needs to

be 2.8 cm^{-1} and 1.4 cm^{-1} respectively. These two values are already smaller than two times (4.6 cm^{-1}) of the largest coupling strength between two adjacent anions in the KSCN crystal. Under such a circumstance, using eq.5 to predict resonant energy transfer can introduce nontrivial uncertainties as the energy transfer can go through the coherent process of which the energy transfer rate only slightly (or don't, under the perfect

condition) depends on the dephasing time.²⁴ As we can see from fig.S2 in SI, the resonant energy transfer only becomes slightly faster ($\sim 30\%$) from room temperature down to 80K. There can be a third possible explanation for the observed huge temperature dependence. According to a previous nonlinear theory of dephasing on energy transfer rates,³⁶⁻³⁸ a more dramatic increase in the energy transfer rate with increasing dephasing rate is expected when the latter is not very large, e.g. at 80K, with a smaller increase at a larger dephasing rate, e.g. 295K. Such an effect can be more dramatic in the 1/1 mixed crystal with a smaller gap (48 cm^{-1}) than in the mixed crystal with a larger gap (75 cm^{-1}).

4.6.3 Nonresonant Vibrational Energy Transfer in Mixed Crystals of KSCN/KS¹³C¹⁵N of Different Ratios

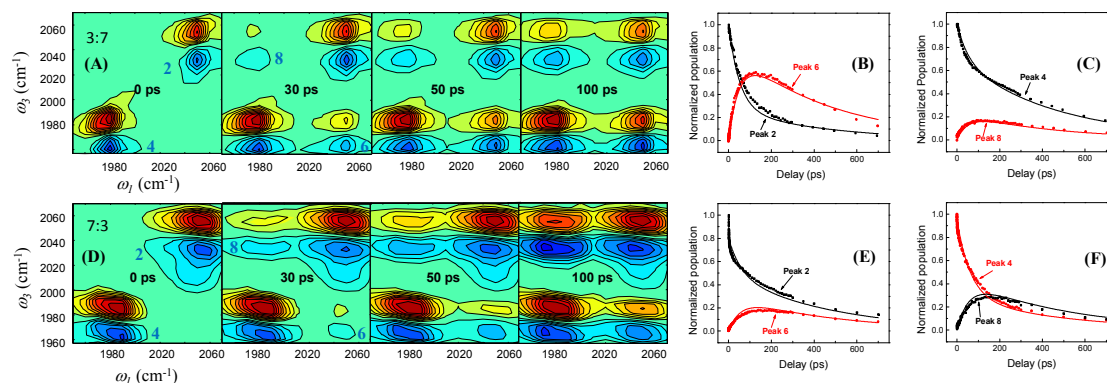


Figure 12. (A) 2D IR spectra of a KSCN/KS¹³C¹⁵N=3/7 mixed crystal at 295K at four waiting times; (B) and (C) the waiting time dependent intensities of peaks 2, 4, 6, 8 in (A). Dots are experimental results, and lines are kinetic model calculations. (D) 2D IR spectra of a KSCN/KS¹³C¹⁵N=7/3 mixed crystal at 295K at four waiting times; (E) and (F) the waiting time dependent intensities of peaks 2, 4, 6, 8 in (D). Dots are experimental results, and lines are kinetic model calculations. In each 2D IR spectrum, the diagonal

peaks are normalized to 1, and the corresponding cross peaks along the y-axis are normalized accordingly.

There can be a concern that in the mixed crystals of KSCN and its isotope-labeled species $^{13}\text{C}^{15}\text{N}$ or the other species can form individual domains so that the energy transfers may not follow the exact molar ratio of the two species. To address this issue, we measured the vibrational energy exchanges (fig.12) in two mixed crystals of KSCN/ $^{13}\text{C}^{15}\text{N}$ with 3/7 and 7/3 molar ratios at room temperature, in addition to the 1/1 sample discussed above. Analyses show that in the KSCN/ $^{13}\text{C}^{15}\text{N}$ =3/7 sample, the CN to $^{13}\text{C}^{15}\text{N}$ energy transfer time is $\frac{1}{k_{\text{CN}\rightarrow^{13}\text{C}^{15}\text{N}}} = 68 \pm 5 \text{ ps}$ and the reverse transfer time is

$\frac{1}{k_{^{13}\text{C}^{15}\text{N}\rightarrow\text{CN}}} = 240 \pm 10 \text{ ps}$. In the KSCN/ $^{13}\text{C}^{15}\text{N}$ =7/3 sample, the CN to $^{13}\text{C}^{15}\text{N}$ energy

transfer time is $\frac{1}{k_{\text{CN}\rightarrow^{13}\text{C}^{15}\text{N}}} = 162 \pm 8 \text{ ps}$ and the reverse transfer time is

$\frac{1}{k_{^{13}\text{C}^{15}\text{N}\rightarrow\text{CN}}} = 104 \pm 5 \text{ ps}$. The transfer forward and backward rate constant ratios in both

samples can be described by the equation

$$\frac{k_{DA}}{k_{AD}} = e^{\frac{E_D - E_A}{RT}} \times \frac{n_A}{n_D}, \quad \text{eq.27}$$

where k_{DA} and k_{AD} are the transfer rate from D to A and from A to D respectively, E_D and E_A are the energy values of D and A respectively, and n_D and n_A are the numbers of D and A. Eq.27 is based on the fact that in a typical nonlinear IR experiment, only less than 5% of the molecules are vibrationally excited by the lasers. Therefore, for a D/A ratio larger than the ratio of molecules that are laser-excited, the relative number of the

energy acceptors for one donor in a series of experiments is only determined by the concentration of the acceptors. For instances, in the three KSCN/KS¹³C¹⁵N mixed samples, the concentrations of S¹³C¹⁵N⁻ are 30% (KSCN/KS¹³C¹⁵N=7/3), 50% (KSCN/KS¹³C¹⁵N=1/1) and 70% (KSCN/KS¹³C¹⁵N=3/7). For the energy transfer from CN to ¹³C¹⁵N, the ratio of the number of energy acceptors in the three samples is 3/5/7. Therefore, the energy transfer time ratio must also be 7/5/3. Experimentally, the ratio is 162/99/68 = 7.1/4.4/3. The experimental ratio is very close to the predicted ratio, indicating that in the mixed crystalline samples the effect of micron domains of single species (if any) on the energy transfer rates is statistically averaged. This result can be explained in another way. The chemical properties of KSCN and its isotope-labeled counterparts are essentially identical, and therefore the probability at any physical location in the sample is the same for each species. This naturally leads to the linear relationship between the number of the acceptors and the concentration of the species other than the donor.

In summary, using the crystalline samples, we were able to quantitatively test the dephasing mechanism with resonant vibrational energy transfers. We were also able to demonstrate two different energy gap dependences of the nonresonant vibrational energy transfers. The observed energy gap dependences and the temperature dependence of vibrational energy transfers of the KSCN/KS¹³C¹⁵N=1/1 mixed crystal can be described by eq.24 of the phonon compensation mechanism reasonably well. The temperature dependence of energy transfers of the KSCN/KS¹³CN=1/1 mixed crystal is probably the sum result of both mechanisms. The dependences are hard to explain by the phonon

compensation mechanism of the first order perturbation approach unless some specific conditions which seem to be less reasonable (compared to those for eq.24) are assumed.

5. Concluding Remarks

In this work, we systematically studied intermolecular vibrational energy transfers in liquids and crystalline solids. We found that in both liquid and solid samples, the resonant energy transfers are faster at a lower temperature but the nonresonant energy transfers are slower at a lower temperature. In liquids, at the same temperature, the nonresonant energy is faster if the donor/acceptor energy gap is smaller. In solids, dependent on the temperature, the nonresonant energy transfers can be faster with a larger donor/acceptor energy gap or energy gap independent. To explain the experimental observations, we proposed two energy transfer mechanisms: the dephasing mechanism which is essentially dependent on the probability of the donor being resonant with the acceptor caused by the dephasing events; and the phonon compensation mechanism of the second order perturbation that is dependent on the environment to provide phonons to compensate the donor/acceptor energy gap. In the first mechanism, the probability of donor/acceptor on resonance physically exists. In the second mechanism, the phonon compensation is through the “virtual intermediate states” which don’t physically exist. The experimental results in the liquid samples and the resonant energy transfer data in the solid samples are well explained by the dephasing mechanism. The quantitative nature of this mechanism also allows the donor/acceptor distance to be derived from the vibrational energy transfer rate measurements (combined with the transition dipole/transition dipole interaction). The nonresonant vibrational energy transfer experiments in the solid samples can be reasonably described by the phonon compensation mechanism. We expect that

both energy transfer mechanisms simultaneously play roles in nonresonant vibrational energy transfers in condensed phases. Which mechanism is dominant is dependent on the detailed situation. Based on our results, our tentative opinion is that since the essential differences in liquid and crystalline solid samples are that in solids there can be many more well defined phonon modes but in liquids the dephasing is typically faster, in liquids the dephasing mechanism is probably dominant if no specific phonon modes exist in the frequency range of the donor/acceptor gap for relatively small gaps (e.g. $\Delta\omega < RT$). In solids, the phonon compensation mechanism can be important in samples where many phonon modes at the donor/acceptor energy gaps exist. One unsatisfactory point of the phonon compensation mechanism is that the phonon/system coupling and the phonon densities involved in the energy transfer process are very difficult to be experimentally obtained. How to solve this issue is subject to future studies.

ASSOCIATED CONTENT

Supporting Information

The calculation parameters of the figures containing kinetic model calculations.

AUTHOR INFORMATION

Corresponding Author

junrong@rice.edu

Notes

The authors declare no competing financial interest

ACKNOWLEDGEMENTS

This material is based upon work supported by the Welch foundation under Award No. C-1752 and AFOSR Award No. FA9550-11-1-0070. J. R. Zheng also thanks the David and Lucile Packard Foundation for a Packard fellowship. Insightful discussions with Profs. Robert, F. Curl, Peter Wolynes, Anatoly B. Kolomeisky, David Jonas, Greg Angel, James Hynes, Wei Yang, Yi-qin Gao, and Zhigang Sun are appreciated.

References

1. D. W. Oxtoby, *Annu. Rev. Phys. Chem.*, 1981, **32**, 77-101.
2. A. Laubereau, L. Kirschner and W. Kaiser, *Opt. Commun.*, 1973, **9**, 182-185.
3. A. Laubereau and W. Kaiser, *Rev. Mod. Phys.*, 1978, **50**, 607.
4. D. W. Oxtoby, *Adv. Chem. Phys.*, 1981, **47**, 487-519.
5. E. L. Sibert, W. P. Reinhardt and J. T. Hynes, *J. Chem. Phys.*, 1984, **81**, 1115-1134.
6. X. Y. Hong, S. Chen and D. D. Dlott, *J. Phys. Chem.*, 1995, **99**, 9102-9109.
7. A. Tokmakoff, B. Sauter and M. D. Fayer, *J. Chem. Phys.*, 1994, **100**, 9035.
8. S. A. Egorov and J. L. Skinner, *J. Chem. Phys.*, 1996, **105**, 7047-7058.
9. H. J. Bakker, *J. Chem. Phys.*, 1993, **98**, 8496.
10. R. M. Stratt, *Accts. of Chem. Res.*, 1995, **28**, 201-207.
11. J. C. Owrtusky, D. Raftery and R. M. Hochstrasser, *Ann. Rev. Phys. Chem.*, 1994, **45**, 519.
12. E. L. Sibert and R. Rey, *J. Chem. Phys.*, 2002, **116**, 237-257.
13. M. Yang, F. Li and J. L. Skinner, *J. Chem. Phys.*, 2011, **135**, 10.
14. J. L. Skinner, *Theor. Chem. Acc.*, 2011, **128**, 147-155.
15. V. M. Kenkre, A. Tokmakoff and M. D. Fayer, *J. Chem. Phys.*, 1994, **101**, 10618-10629.
16. H. T. Bian, X. W. Wen, J. B. Li and J. R. Zheng, *J. Chem. Phys.*, 2010, **133**, 034505.
17. H. Bian, J. Li, X. Wen and J. R. Zheng, *J. Chem. Phys.*, 2010, **132**, 184505.
18. H. T. Bian, H. L. Chen, J. B. Li, X. W. Wen and J. R. Zheng, *J. Phys. Chem. A.*, 2011, **115**, 11657-11664.
19. H. T. Bian, X. W. Wen, J. B. Li, H. L. Chen, S. Z. Han, X. Q. Sun, J. A. Song, W. Zhuang and J. R. Zheng, *Proc. Natl. Acad. Sci. U. S. A.*, 2011, **108**, 4737-4742.
20. H. T. Bian, J. B. Li, Q. Zhang, H. L. Chen, W. Zhuang, Y. Q. Gao and J. R. Zheng, *J. Phys. Chem. B*, 2012, **116**, 14426-14432.

21. J. B. Li, H. T. Bian, X. W. Wen, H. L. Chen, K. J. Yuan and J. R. Zheng, *J. Phys. Chem. B.*, 2012, **116**, 12284-12294.
22. J. B. Li, H. T. Bian, H. L. Chen, B. Hoang and J. R. Zheng, *J. Phys. Chem. B.*, 2013, **117**, 4274 - 4283.
23. D. Laage, H. Demirdjian and J. T. Hynes, *Chem. Phys. Lett.*, 2005, **405**, 453-458.
24. J. A. Leegwater, *J. Phys. Chem.*, 1996, **100**, 14403-14409.
25. H. L. Chen, H. T. Bian, J. B. Li, X. M. Guo, X. W. Wen and J. R. Zheng, *J. Phys. Chem. B.*, 2013, **117**, 15614-15624.
26. T. Förster, *Ann. Phys. Leipzig*, 1948, **2**, 55.
27. D. L. Dexter, *J. Chem. Phys.*, 1953, **21**, 836-850.
28. T. Miyakawa and D. L. Dexter, *Phys. Rev. B*, 1970, **1**, 2961-2969.
29. A. Nitzan and R. J. Silbey, *J. Chem. Phys.*, 1974, **60**, 4070-4075.
30. Rackovsk.S and R. Silbey, *Mol. Phys.*, 1973, **25**, 61-72.
31. A. Nitzan, S. Mukamel and J. Jortner, *J. Chem. Phys.*, 1975, **63**, 200-207.
32. T. Holstein, S. K. Lyo and R. Orbach, in *Laser spectroscopy of solids*, Springer, New York, 1986, pp. 39-82.
33. A. A. Stuchebrukhov and R. A. Marcus, *J. Chem. Phys.*, 1993, **98**, 6044-6061.
34. S. H. Lin, *J. Chem. Phys.*, 1976, **65**, 1053-1062.
35. S. A. Egorov and J. L. Skinner, *J. Chem. Phys.*, 1995, **103**, 1533-1543.
36. D. E. Logan and P. G. Wolynes, *The Journal of chemical physics*, 1990, **93**, 4994-5012.
37. D. E. Logan and P. G. Wolynes, *The Journal of chemical physics*, 1987, **87**, 7199-7207.
38. D. M. Leitner, *New Journal of Physics*, 2010, **12**, 085004.
39. R. F. Curl, J. V. V. Kasper and K. S. Pitzer, *J. Chem. Phys.*, 1967, **46**, 3220-3228.
40. H. L. Chen, X. W. Wen, J. B. Li and J. R. Zheng, *J. Phys. Chem. A.*, 2014, **118**, 2463-2469.
41. J. Zheng, K. Kwak and M. D. Fayer, *Acc. of Chem. Res.*, 2007, **40**, 75-83.
42. J. Zheng, K. Kwak, J. B. Asbury, X. Chen, I. Piletic and M. D. Fayer, *Science*, 2005, **309**, 1338-1343.
43. J. Zheng and M. D. Fayer, *J. Phys. Chem. B.*, 2008, **112**, 10221.
44. O. Golonzka, M. Khalil, N. Demirdoven and A. Tokmakoff, *Phys. Rev. Lett.*, 2001, **86**, 2154-2157.
45. M. Khalil, N. Demirdoven and A. Tokmakoff, *J. Phys. Chem. A.*, 2003, **107**, 5258-5279.
46. Y. S. Kim and R. M. Hochstrasser, *Proc. Natl. Acad. Sci.*, 2005, **102**, 11185-11190.
47. S. A. Egorov and B. J. Berne, *J. Chem. Phys.*, 1997, **107**, 6050-6061.
48. R. Zwanzig, *J. Chem. Phys.*, 1961, **34**, 1931-1935.
49. H. L. Chen, H. T. Bian, J. B. Li, X. W. Wen and J. R. Zheng, *Inter. Rev. Phys. Chem.*, 2012, **31**, 469-565.
50. G. D. Scholes, *Annu. Rev. Phys. Chem.*, 2003, **54**, 57-87.
51. J. C. Chang, *J. Chem. Phys.*, 1977, **67**, 3901-3909.
52. S. Woutersen and H. J. Bakker, *Nature*, 1999, **402**, 507-509.
53. I. Natkaniec, L. S. Smirnov and A. I. Solovev, *Physica B*, 1995, **213**, 667-668.

54. H. T. Bian, H. L. Chen, Q. Zhang, J. B. Li, X. W. Wen, W. Zhuang and J. R. Zheng, *J. Phys. Chem. B.*, 2013, **117**, 7972 - 7984.
55. C. Akers, S. W. Peterson and R. D. Willett, *Acta Crystallographica Section B-Structural Crystallography and Crystal Chemistry*, 1968, **B 24**, 1125-1126.
56. D. J. Cookson, M. M. Elcombe and T. R. Finlayson, *Journal of Physics-Condensed Matter*, 1992, **4**, 7851-7864.
57. L. S. Smirnov, I. Natkaniec, Y. A. Shadrin and A. I. Solov'EV, *Acta Phys. Hung.*, 1994, **75**, 275 - 278.